



CHORUS

This is the accepted manuscript made available via CHORUS. The article has been published as:

Large Deformations of a Soft Porous Material

Christopher W. MacMinn, Eric R. Dufresne, and John S. Wettlaufer

Phys. Rev. Applied **5**, 044020 — Published 29 April 2016

DOI: [10.1103/PhysRevApplied.5.044020](https://doi.org/10.1103/PhysRevApplied.5.044020)

Large deformations of a soft porous material

Christopher W. MacMinn,^{1,*} Eric R. Dufresne,² and John S. Wettlaufer^{1,2,3}

¹*University of Oxford, Oxford, UK*

²*Yale University, New Haven, CT, USA*

³*Nordita, Royal Institute of Technology and Stockholm University, Stockholm, Sweden*

Compressing a porous material will decrease the volume of the pore space, driving fluid out. Similarly, injecting fluid into a porous material can expand the pore space, distorting the solid skeleton. This poromechanical coupling has applications ranging from cell and tissue mechanics to geomechanics and hydrogeology. The classical theory of linear poroelasticity captures this coupling by combining Darcy’s law with Terzaghi’s effective stress and linear elasticity in a linearized kinematic framework. This is a good model for very small deformations, but it becomes increasingly inappropriate for moderate to large deformations, which are common in the context of phenomena such as swelling and damage, and for soft materials such as gels and tissues. The well-known theory of large-deformation poroelasticity combines Darcy’s law with Terzaghi’s effective stress and nonlinear elasticity in a rigorous kinematic framework. This theory has been used extensively in biomechanics to model large elastic deformations in soft tissues, and in geomechanics to model large elasto-plastic deformations in soils. Here, we first provide an overview and discussion of this theory with an emphasis on the physics of poromechanical coupling. We present the large-deformation theory in an Eulerian framework to minimize the mathematical complexity, and we show how this simplifies to linear poroelasticity under the assumption of small strain. We then compare the predictions of linear poroelasticity with those of large-deformation poroelasticity in the context of two uniaxial model problems: Fluid outflow driven by an applied mechanical load (the consolidation problem) and compression driven by a steady fluid through-flow. We explore the steady and dynamical errors associated with the linear model in both situations, as well as the impact of introducing a deformation-dependent permeability. We show that the error in linear poroelasticity is due primarily to kinematic nonlinearity, and that this error (i) plays a surprisingly important role in the dynamics of the deformation and (ii) is amplified by nonlinear constitutive behavior, such as deformation-dependent permeability.

I. INTRODUCTION

In a deformable porous material, deformation of the solid skeleton is mechanically coupled to flow of the interstitial fluid(s). This poromechanical coupling has relevance to problems as diverse as cell and tissue mechanics [*e.g.*, 1–9], magma/mantle dynamics [*e.g.*, 10–15], and hydrogeology [*e.g.*, 16–25]. These problems are notoriously difficult due to the inherently two-way nature of poromechanical coupling, where deformation drives flow and vice-versa.

In poroelasticity, the mechanics of the solid skeleton are described by elasticity theory. The theory of poroelasticity has a rich and interdisciplinary history [26]. Wang [17] provides an excellent discussion of the historical roots of linear poroelasticity, which models poroelastic loading under infinitesimal deformations. Major touchstones in the development of linear poroelasticity include the works of M. A. Biot [*e.g.*, 27–29], who formalized the linear theory and provided a variety of analytical solutions through analogy with thermoelasticity, as well as that of Rice and Cleary [30], who reformulated the linear theory in terms of more tangible material parameters and derived solutions to several model problems.

When the deformation of the skeleton is not in-

finitesimal, poroelasticity must be cast in the framework of large-deformation elasticity [*e.g.*, 31, 32]. Large-deformation poroelasticity has found extensive application over the past few decades in computational biomechanics for the study of soft tissues, which are porous, fluid-saturated, and can accommodate large deformations reversibly. Much of this effort has been directed at capturing the complex and varied structure and constitutive behavior of biological materials [*e.g.*, 33–39]. Large-deformation poroelasticity has also been applied in computational geomechanics for the study of soils and other geomaterials. Soils typically accommodate large deformations through ductile failure (plasticity or yielding) due to their granular and weakly cemented microstructure, and much of the effort has been directed at the challenges of large-deformation elasto-plasticity [*e.g.*, 40–43]. Large deformations can also occur through swelling [*e.g.*, 44, 45], which has attracted interest recently in the context of gels [*e.g.*, 46–48].

Large-deformation (poro)elasticity is traditionally approached almost exclusively with computational tools, and these are based almost exclusively on the finite-element method and in a Lagrangian framework [*e.g.*, 46, 48]. A thorough treatment of the Lagrangian approach to large-deformation poroelasticity can be found in Ref. [32]. Although powerful, these tools can be cumbersome from the perspective of developing physical insight. They are also poorly suited for studying nontrivial flow and solute transport through the pore structure.

* christopher.macminn@eng.ox.ac.uk

Here, we instead consider the general theory of large-deformation poroelasticity in an Eulerian framework. Although the Eulerian approach is well known [*e.g.*, 32], it has very rarely been applied to practical problems and a clear and unified presentation is lacking. This approach is useful in the present context to clearly emphasize the physics of poromechanical coupling.

In the first part of this paper, we review and discuss the well-known theory (§II–III). We first consider the exact description of the kinematics of flow and deformation, adopting a simple but nonlinear elastic response in the solid skeleton (§II). We then show how this theory reduces to linear poroelasticity in the limit of infinitesimal deformations (§III).

In the second part of this paper, we compare the linear and large-deformation theories in the context of two uniaxial model problems (§IV–VI). The primary goals of this comparison are to study the role of kinematic nonlinearity in large deformations, and to examine the resulting error in the linear theory. The two model problems are: (i) Compression driven by an applied load (the consolidation problem) and (ii) compression driven by a net fluid through-flow. In the former, the evolution of the deformation is controlled by the rate at which fluid is squeezed through the material and out at the boundaries; as a result, fluid flow is central to the rate of deformation but plays no role in the steady state. In the latter, fluid flow is also central to the steady state since this is set by the steady balance between the gradient in fluid pressure and the gradient in stress within the solid skeleton. We show that, in both cases, the error in linear poroelasticity due to the missing kinematic nonlinearities plays a surprisingly important role in the dynamics of the deformation, and that this error is amplified by nonlinear constitutive behavior such as deformation-dependent permeability.

II. LARGE-DEFORMATION POROELASTICITY

Poroelasticity is a multiphase theory in that it describes the coexistence and interaction of multiple immiscible constituent materials, or phases [*e.g.*, 49]. Here, we restrict ourselves to two phases: A solid and a fluid. The solid phase is arranged into a porous and deformable macroscopic structure, “the solid skeleton” or “the skeleton”, and the pore space of the solid skeleton is saturated with a single interstitial fluid. Deformation of the solid skeleton leads to rearrangement of its pore structure, with corresponding changes in the local volume fractions (see §II B). Throughout, we use the terms “the solid grains” or “the solid” to refer to the solid phase and “the interstitial fluid” or “the fluid” to refer to the fluid phase. Although the term “grain” is inappropriate in the context of porous materials with fibrous microstructure, such as textiles, polymeric gels, or tissues, we use it generically for convenience.

We assume here that the two constituent materials are incompressible, meaning that the mass densities of the

fluid, ρ_f , and of the solid, ρ_s , are constant. Note that this does not prohibit compression of the solid skeleton—variations in the macroscopic mass density of the porous material are enabled by changes in its pore volume. The assumption of incompressible constituents is standard in soil mechanics and biomechanics, where fluid pressures and solid stresses are typically very small compared to the bulk moduli of the constituent materials. However, some caution is merited in the context of deep aquifers where, at a depth of a few kilometers, the hydrostatic pressure and lithostatic stress themselves approach a few percent of the bulk moduli of water and mineral grains. In these cases, it may be appropriate to allow for fluid compressibility while retaining the incompressibility of the solid grains, in which case much of the theory discussed here still applies. The theory of poroelasticity can be generalized to allow for compressible constituents [*e.g.*, 17, 32, 50–52], but this is beyond the scope of this paper.

What follows is, in essence, a brief and superficial introduction to continuum mechanics in the context of a porous material. We have minimized the mathematical complexity where possible for the sake of clarity, and to preserve an emphasis on the fundamental physics. For the more mathematically inclined reader, excellent resources are available for further study [*e.g.*, 32, 53, 54].

A. Eulerian and Lagrangian reference frames

A core concept in continuum mechanics is the distinction between a Lagrangian reference frame (fixed to the material) and an Eulerian one (fixed in space). These two perspectives are rigorously equivalent, so the choice is purely a matter of convention and convenience. A Lagrangian frame is the natural and traditional choice in solid mechanics, where displacements are typically small and where the current state of stress is always tied to the reference (undeformed) configuration of the material through the current state of strain (displacement gradients). An Eulerian frame is the natural and traditional choice in fluid mechanics, where displacements are typically large and where the current state of stress depends only on the instantaneous rate of strain (velocity gradients). More complex materials such as viscoelastic solids and non-Newtonian fluids can have elements of both, with a dependence on both strain and strain rate [*e.g.*, 55, 56].

Problems involving fluid-solid coupling lead to a clear conflict between the Eulerian and Lagrangian approaches. In classical fluid-structure interaction problems, such as air flow around a flapping flag or blood flow through an artery, the fluid and the solid exist in separate domains that are coupled along a shared moving boundary. In a porous material, in contrast, the fluid and the solid coexist in the same domain and are coupled through bulk conservation laws. As a result, the entire problem must be posed either in a fixed Eulerian frame

or in a Lagrangian frame attached to the solid skeleton. One major advantage of the latter approach is that it eliminates moving (solid) boundaries since the skeleton is stationary relative to a Lagrangian coordinate system; this is particularly powerful and convenient in the context of computation. However, the Eulerian approach leads to a simpler and more intuitive mathematical model in the context of fluid flow and transport, and it is straightforward and even advantageous when boundary motion is absent or geometrically simple. This conflict can be avoided altogether when the deformation of the skeleton is small, such that the distinction between an Eulerian frame and a Lagrangian one can be ignored; this is a core assumption of linear (poro)elasticity.

In the present context, we consider two model problems where the fluid and the skeleton are tightly coupled, the deformation of the skeleton is large, and there is a moving boundary. We pose these problems fully in an Eulerian frame and write all quantities as functions of an Eulerian coordinate \mathbf{x} , fixed in the laboratory frame. Accordingly, we adopt the notation

$$\nabla \equiv \hat{e}_i \frac{\partial}{\partial x_i}, \quad (1)$$

where the x_i are the components of the Eulerian coordinate system, $i = 1, 2, 3$, with \hat{e}_i the associated unit vectors, and adopting the Einstein summation convention. For reference and comparison, we summarize the key aspects of the Lagrangian framework in Appendix A.

B. Volume fractions

We denote the local volume fractions of fluid and solid by ϕ_f (the porosity, fluid fraction, or void fraction) and ϕ_s (the solid fraction), respectively. These are the *true* volume fractions in the sense that they measure the current phase volume per unit current total volume, such that $\phi_f + \phi_s \equiv 1$. As such, the true porosity is the relevant quantity for calculating flow and transport through the pore structure. However, changes in ϕ_f at a spatial point \mathbf{x} reflect both deformation and motion of the underlying skeleton, so the relevant state of stress must be calculated with some care.

Alternatively, it is possible to define *nominal* volume fractions that measure the current phase volume per unit reference total volume [32]. These are convenient in a Lagrangian frame where, if the solid phase is incompressible, the nominal solid fraction is constant by definition and the nominal porosity is linearly related to the local volumetric strain. However, the nominal porosity is not directly relevant to flow and transport. In addition, the nominal volume fractions do not sum to unity; rather, they must sum to the Jacobian determinant J (see §II C). Here, we avoid these nominal quantities and work strictly with the true porosity. Note that Coussy [32] denotes the true porosity (“Eulerian porosity”) by n and the nominal porosity (“Lagrangian porosity”) by ϕ , whereas we

denote the true porosity by ϕ_f and the nominal porosity by Φ_f (see Appendix A).

C. Kinematics of solid deformation

The most primitive quantity for calculating deformation is the displacement field, which is a map between the current configuration of the solid skeleton and its reference configuration. In other words, the displacement field measures the displacement of material points from their reference positions. In an Eulerian frame, the solid displacement field $\mathbf{u}_s(\mathbf{x}, t)$ is given by

$$\mathbf{u}_s(\mathbf{x}, t) = \mathbf{x} - \mathbf{X}(\mathbf{x}, t), \quad (2)$$

where \mathbf{X} is the reference position of the material point that sits at position \mathbf{x} at time t (*i.e.*, it is the Lagrangian coordinate in our Eulerian frame). We adopt the convention that $\mathbf{X}(\mathbf{x}, 0) = \mathbf{x}$ such that $\mathbf{u}_s(\mathbf{x}, 0) = 0$; this is not required, but it simplifies the analysis.

The displacement field is not directly a measure of deformation because it includes rigid-body motions. The deformation-gradient tensor \mathbf{F} , which is the Jacobian of the deformation field, excludes translations by considering the spatial gradient of the displacement field. In an Eulerian frame, \mathbf{F} is more readily defined through its inverse,

$$\mathbf{F}^{-1} = \nabla \mathbf{X} = \mathbf{I} - \nabla \mathbf{u}_s, \quad (3)$$

where $(\cdot)^{-1}$ denotes the inverse and \mathbf{I} is the identity tensor. The deformation-gradient tensor \mathbf{F} still includes rigid-body rotations, but these can be excluded by multiplying \mathbf{F} by its transpose. Hence, measures of strain are ultimately derived from the right Cauchy-Green deformation tensor $\mathbf{C} = \mathbf{F}^T \mathbf{F}$ or the left Cauchy-Green deformation tensor $\mathbf{B} = \mathbf{F} \mathbf{F}^T$, where $(\cdot)^T$ denotes the transpose.

The eigenvalues λ_i^2 of \mathbf{C} (or, equivalently, of \mathbf{B}) are the squares of the principal stretches λ_i , with $i = 1, 2, 3$. The stretches measure the amount of elongation along the principal axes of the deformation, which are themselves related to the eigenvectors of \mathbf{C} and \mathbf{B} : In the reference configuration, they are the normalized eigenvectors of \mathbf{C} ; in the current configuration, they are the normalized eigenvectors of \mathbf{B} .

The Jacobian determinant J measures the amount of local volume change during the deformation,

$$J(\mathbf{x}, t) = \det(\mathbf{F}) = \frac{1}{\det(\mathbf{F}^{-1})} = \lambda_1 \lambda_2 \lambda_3. \quad (4)$$

This is precisely the ratio of the current volume of the material at point \mathbf{x} to its reference volume, and where $\det(\cdot)$ denotes the determinant. For an incompressible solid skeleton, $J \equiv 1$. For a compressible solid skeleton made up of incompressible solid grains, as considered here, deformation occurs strictly through rearrangement

of the pore structure and the Jacobian determinant is connected directly to the porosity,

$$J(\mathbf{x}, t) = \frac{1 - \phi_{f,0}(\mathbf{x}, t)}{1 - \phi_f(\mathbf{x}, t)}, \quad (5)$$

where $\phi_{f,0}(\mathbf{x}, t) \equiv \phi_f(\mathbf{x} - \mathbf{u}_s(\mathbf{x}, t), 0)$ is the reference porosity field. In an Eulerian frame, the reference porosity field depends on \mathbf{u}_s because it refers to the initial porosity of the material that is currently located at \mathbf{x} but that was originally located at $\mathbf{x} - \mathbf{u}_s$. Note that $\phi_{f,0}(\mathbf{x}, t) \neq \phi_f(\mathbf{x}, 0)$ unless $\phi_f(\mathbf{x}, 0)$ is spatially uniform, in which case $\phi_f(\mathbf{x}, 0) = \phi_{f,0}$ is simply a constant and this distinction is unimportant.

Lastly, local continuity for the incompressible solid phase is written

$$\frac{\partial \phi_s}{\partial t} + \nabla \cdot (\phi_s \mathbf{v}_s) = 0 \quad \text{or} \quad \frac{\partial \phi_f}{\partial t} - \nabla \cdot [(1 - \phi_f) \mathbf{v}_s] = 0, \quad (6)$$

where $\mathbf{v}_s(\mathbf{x}, t)$ is the solid velocity field. The solid velocity is the material derivative of the solid displacement,

$$\mathbf{v}_s = \frac{D\mathbf{u}_s}{Dt} \equiv \frac{\partial \mathbf{u}_s}{\partial t} + \mathbf{v}_s \cdot \nabla \mathbf{u}_s = \frac{\partial \mathbf{u}_s}{\partial t} \cdot \mathbf{F}. \quad (7)$$

Equations (2)–(7) provide an exact kinematic description of the deformation of the solid skeleton, assuming only that the solid phase is incompressible. This is valid for arbitrarily large deformations and, because it is simply a geometric description of the changing pore space, it *makes no assumptions about the fluid that occupies the pore space*. This remains rigorously valid when the fluid phase is compressible, and in the presence of multiple fluid phases. Further, this description *makes no additional assumptions about the constitutive behavior of the solid skeleton*—it remains rigorously valid for any elasticity law, and in the presence of viscous dissipation or plasticity.

D. Kinematics of fluid flow

We assume that the pore space of the solid skeleton is saturated with a single fluid phase. For a compressible fluid phase, local continuity is written

$$\frac{\partial}{\partial t} (\rho_f \phi_f) + \nabla \cdot (\rho_f \phi_f \mathbf{v}_f) = 0, \quad (8)$$

where $\mathbf{v}_f(\mathbf{x}, t)$ is the fluid velocity field. This remains valid for multiple fluid phases if ρ_f and \mathbf{v}_f are calculated as fluid-phase-averaged quantities, in which case Equation (8) must also be supplemented by a conservation law for each of the individual fluid phases. For simplicity, we focus here on the case of a single, incompressible fluid phase, for which we have

$$\frac{\partial \phi_f}{\partial t} + \nabla \cdot (\phi_f \mathbf{v}_f) = 0. \quad (9)$$

There is no need to introduce a fluid displacement field since we assume below that the fluid is Newtonian. The constitutive law for a Newtonian fluid, and also for many non-Newtonian fluids, depends only on the fluid velocity.

E. Constitutive laws for fluid flow

We assume that the fluid flows relative to the solid skeleton according to Darcy's law. For a single Newtonian fluid, Darcy's law can be written

$$\phi_f (\mathbf{v}_f - \mathbf{v}_s) = -\frac{k(\phi_f)}{\mu} (\nabla p - \rho_f \mathbf{g}), \quad (10)$$

where $k(\phi_f)$ is the permeability of the solid skeleton, which we have taken to be an isotropic function of porosity only, μ is the dynamic viscosity of the fluid, \mathbf{g} is the body force per unit mass due to gravity, and we have neglected body forces other than gravity.

Darcy's law is an implicit statement about the continuum-scale form of the mechanical interactions between the fluid and solid [*e.g.*, §3.3.1 of 32]. We simply adopt it here as a phenomenological model for flow of a single fluid through a porous material. In the presence of multiple fluid phases, Equation (10) can be replaced by the classical multiphase extension of Darcy's law [*e.g.*, 57]. For a single but non-Newtonian fluid phase, Equation (10) must be modified accordingly [*e.g.*, 58].

Generally, the permeability will change with the pore structure as the skeleton deforms, although this dependence is neglected in linear poroelasticity, where it is assumed that deformations are infinitesimal. The simplest representation of this is to take the permeability to be a function of the porosity, as we have done above, and here again the true porosity is the relevant quantity. A common choice is the Kozeny-Carman formula, one form of which is

$$k(\phi_f) = \frac{d^2}{180} \frac{\phi_f^3}{(1 - \phi_f)^2}, \quad (11)$$

where d is the typical pore or grain size. This was derived from experimental measurements in beds of close-packed spheres, but is commonly used for a wide range of materials. One reason for this is that the Kozeny-Carman formula respects two physical limits that are important for poromechanics: The permeability vanishes as the porosity vanishes, and diverges as the porosity approaches unity. The former requirement ensures that fluid flow cannot drive the porosity below zero, and the latter prevents the flow from driving the porosity above unity.

We use a normalized Kozeny-Carman formula here,

$$k(\phi_f) = k_0 \frac{(1 - \phi_{f,0})^2}{\phi_{f,0}^3} \frac{\phi_f^3}{(1 - \phi_f)^2}, \quad (12)$$

where $k(\phi_{f,0}) = k_0$ is the relaxed/undeformed permeability. This preserves the qualitative characteristics of the

original relationship while allowing the initial permeability and the initial porosity to be imposed independently. Clearly, it is straightforward to design other permeability laws that have the same characteristics. Note that the particular choice of permeability law will dominate the flow and mechanics in the limit of vanishing permeability since the pressure gradient, which is coupled with the solid mechanics, is inversely proportional to the permeability.

Since porosity is strictly volumetric, writing $k = k(\phi_f)$ neglects the impacts of rotation and shear. This is overly simplistic for materials with inherently anisotropic permeability fields, the axes of which would rotate under rigid-body rotation and would be distorted in shear. It is also possible that permeability anisotropy could emerge through anisotropic deformations, or through other effects creating orthotropic structure. We neglect these effects here for simplicity.

F. Nonlinear flow equation

One convenient way of combining Equations (6), (9), and (10) is by defining the total volume flux \mathbf{q} as

$$\mathbf{q} \equiv \phi_f \mathbf{v}_f + (1 - \phi_f) \mathbf{v}_s. \quad (13)$$

This measures the total volume flow per unit total cross-sectional area per unit time. The total flux can also be viewed as a phase-averaged, composite, or bulk velocity. From this, it is then straightforward to derive

$$\frac{\partial \phi_f}{\partial t} + \nabla \cdot \left[\phi_f \mathbf{q} - (1 - \phi_f) \frac{k(\phi_f)}{\mu} (\nabla p - \rho_f \mathbf{g}) \right] = 0, \quad (14a)$$

$$\text{and} \quad \nabla \cdot \mathbf{q} = 0, \quad (14b)$$

with

$$\mathbf{v}_f = \mathbf{q} - \left(\frac{1 - \phi_f}{\phi_f} \right) \frac{k(\phi_f)}{\mu} (\nabla p - \rho_f \mathbf{g}), \quad (15a)$$

$$\text{and} \quad \mathbf{v}_s = \mathbf{q} + \frac{k(\phi_f)}{\mu} (\nabla p - \rho_f \mathbf{g}). \quad (15b)$$

Equations (14) and (15) embody Darcy's law and the kinematics of the deformation, describing the coupled relative motion of the fluid and the solid skeleton. It remains to enforce mechanical equilibrium, and to provide a constitutive relation between stress and deformation within the solid skeleton.

G. Mechanical equilibrium

Mechanical equilibrium requires that the fluid and the solid skeleton must jointly support the local mechanical load, and this provides the fundamental poromechanical coupling. The total stress $\boldsymbol{\sigma}$ is the total force supported

by the two-phase system per unit area, and can be written

$$\boldsymbol{\sigma} = (1 - \phi_f) \boldsymbol{\sigma}_s + \phi_f \boldsymbol{\sigma}_f, \quad (16)$$

where $\boldsymbol{\sigma}_s$ and $\boldsymbol{\sigma}_f$ are the solid stress and the fluid stress, respectively. The solid stress is the force supported by the solid per unit solid area, and $(1 - \phi_f) \boldsymbol{\sigma}_s$ is then the force supported by the solid per unit total area. Similarly, the fluid stress is the force supported by the fluid per unit fluid area, and $\phi_f \boldsymbol{\sigma}_f$ is then the force supported by the fluid per unit total area. Note that it is implicitly assumed here and elsewhere that the phase area fractions are equivalent to the phase volume fractions.

Any stress tensor can be decomposed into isotropic (volumetric) and deviatoric (shear) components without loss of generality. For a fluid within a porous solid, it can be shown that the shear component of the stress is negligible relative to the volumetric component at the continuum scale [*e.g.*, §3.3.1 of 32], so that $\boldsymbol{\sigma}_f = -p\mathbf{I}$, where $p \equiv -(1/3)\text{tr}(\boldsymbol{\sigma}_f)$ is the fluid pressure with $\text{tr}(\cdot)$ the trace. Note that we have adopted the sign convention from solid mechanics that tension is positive and compression negative. The opposite convention is usually used in soil mechanics, rock mechanics, and geomechanics since geomaterials are almost always in compression.

Because the fluid permeates the solid skeleton, the solid stress must include an isotropic and compressive component in response to the fluid pressure. This is present even when the fluid is at rest, and/or when the skeleton carries no external load, but this component cannot contribute to deformation unless the solid grains are compressible. Subtracting this component from the solid stress leads to Terzaghi's effective stress $\boldsymbol{\sigma}'$ [59],

$$\boldsymbol{\sigma}' \equiv (1 - \phi_f)(\boldsymbol{\sigma}_s + p\mathbf{I}), \quad (17)$$

which is the force per unit total area supported by the solid skeleton through deformation [*e.g.*, 17, 27, 32, 59]. We can then rewrite Equation (16) in its more familiar form,

$$\boldsymbol{\sigma} = \boldsymbol{\sigma}' - p\mathbf{I}, \quad (18)$$

which can be modified to allow for compressibility of the solid grains [*e.g.*, 52, 60].

Neglecting inertia, and in the absence of body forces other than gravity, mechanical equilibrium then requires that

$$\nabla \cdot \boldsymbol{\sigma} = \nabla \cdot \boldsymbol{\sigma}' - \nabla p = -\rho \mathbf{g}, \quad (19)$$

where $\rho \equiv \phi_f \rho_f + (1 - \phi_s) \rho_s$ is the phase-averaged, composite, or bulk density. A useful but non-rigorous physical interpretation of Equation (19) is that the fluid pressure gradient acts as a body force within the solid skeleton.

The stress tensors in Equation (19) are Cauchy or *true* stresses. These are Eulerian quantities, and Equation (19) is an Eulerian statement: *The current forces on current areas in the current configuration must balance.*

H. Constitutive law for the solid skeleton

We assume that the solid skeleton is an elastic material, for which the state of stress depends on the displacement of material points from a relaxed reference state. This distinguishes the theory of poroelasticity from, for example, the poroviscous framework traditionally used in magma/mantle dynamics, where the skeleton is assumed to behave as a viscous fluid over geophysical timescales [*e.g.*, 13]. This assumption greatly simplifies the mathematical framework for large deformations by eliminating any dependence on displacement, but we cannot take advantage of it here.

The constitutive law for an elastic solid skeleton typically links the effective stress to the solid displacement via an appropriate measure of strain or strain energy. For large deformations, elastic behavior is nonlinear for two reasons. First, the kinematics are inherently nonlinear because the geometry of the body evolves with the deformation (kinematic nonlinearity). Second, most materials harden or soften under large strains as their internal microstructure evolves—that is, the material properties change with the deformation (material or constitutive nonlinearity).

To capture the kinematic nonlinearities introduced by the evolving geometry, relevant measures of finite strain are typically derived from one of the Cauchy-Green deformation tensors. A wide variety of finite-strain measures exist, each of which is paired with an appropriate measure of stress through a stress-strain constitutive relation that includes at least two elastic parameters. In modern hyperelasticity theory, this constitutive relation takes the form of a strain-energy density function. Selection of an appropriate constitutive law and subsequent tuning of the elastic parameters can ultimately match a huge variety of material behaviors, but our focus here is simply on capturing kinematic nonlinearity. For this purpose, we consider a simple hyperelastic model known as Hencky elasticity.

The key idea in Hencky elasticity is to retain the classical strain-energy density function of linear elasticity, but replacing the infinitesimal strain with the Hencky strain [61, 62]. Hencky strain, also known “natural strain” or “true strain”, is an extension to three dimensions of the one-dimensional concept of logarithmic strain. Hencky elasticity is a generic model in that it does not account for material-specific constitutive nonlinearity, but it captures the full geometric nonlinearity of large deformations and thus provides a good model for the elastic behavior of a wide variety of materials under moderate to large deformations [61, 63]. It is also very commonly used in large-deformation plasticity. Hencky strain has some computational disadvantages [64], but these are not relevant here.

Hencky elasticity can be written

$$J\boldsymbol{\sigma}' = \Lambda \operatorname{tr}(\mathbf{H})\mathbf{I} + (\mathcal{M} - \Lambda)\mathbf{H}, \quad \text{and} \quad (20a)$$

$$\mathbf{H} = \frac{1}{2} \ln(\mathbf{F}\mathbf{F}^\top), \quad (20b)$$

where \mathbf{H} is the Hencky strain tensor and the J on the left-hand side of Equation (20a) accounts for volume change during the deformation. Hencky elasticity reduces to linear elasticity for small strains and, conveniently, it uses the same elastic parameters as linear elasticity (see §III). For compactness, we work in terms of the oedometric or p -wave modulus $\mathcal{M} = \mathcal{K} + \frac{4}{3}\mathcal{G}$ and Lamé’s first parameter $\Lambda = \mathcal{K} - \frac{2}{3}\mathcal{G}$, where \mathcal{K} and \mathcal{G} are the bulk modulus and shear modulus of the solid skeleton, respectively. Note that Lamé’s first parameter is often denoted λ , but we use Λ here to avoid confusion with the principal stretches λ_i . All of these elastic moduli are “drained” properties, meaning that they are mechanical properties of the solid skeleton alone and must be measured under quasi-static conditions where the fluid is allowed to drain (leave) or enter freely.

I. Boundary conditions

Poromechanics describes flow and deformation within a porous material, so the boundaries of the spatial domain typically coincide with the boundaries of the solid skeleton. These boundaries may move as the skeleton deforms; in an Eulerian framework, this constitutes a moving-boundary problem. This is the primary disadvantage of working in an Eulerian framework as it can be analytically and numerically inconvenient. One noteworthy exception is in infinite or semi-infinite domains, in which case suitable far-field conditions are applied; this is common in geophysical problems, which are often spatially extensive.

To close the model presented above, we require kinematic and dynamic boundary conditions for the fluid and the skeleton. Kinematic conditions are straightforward: For the fluid, the most common kinematic conditions are constraints on the flux through the boundaries; for the solid, kinematic conditions typically enforce that the boundaries of the domain are *material* boundaries, meaning that they move with the skeleton.

The simplest dynamic conditions are an imposed total stress, an imposed effective stress, or an imposed fluid pressure. At a permeable boundary, any two of these three quantities can be imposed. At an unconstrained permeable boundary, for example, the normal component of the total stress will come from the fluid pressure and the shear component must vanish; this then implies that both the normal and shear components of the effective stress must vanish. At an impermeable boundary, in contrast, only the total stress can be imposed—the decomposition of the load into fluid pressure and effective stress within the domain will arise naturally through the

solution of the problem (although imposed shear stress can only be supported by the solid skeleton, via effective stress). Some care is required with more complex dynamic conditions that provide coupling with a non-Darcy external flow [*e.g.*, 65–67], but this is beyond the scope of this paper.

III. LINEAR POROELASTICITY

We now briefly derive the theory of linear poroelasticity by considering the limit of infinitesimal deformations. For a deformation characterised by typical displacements of size $\delta \sim \|\mathbf{u}_s\|$ varying over spatial scales of size $\mathcal{L} \sim \|\mathbf{x}\| \sim \|\mathbf{X}\|$, the characteristic strain is of size $\epsilon \equiv \delta/\mathcal{L} \sim \|\nabla \mathbf{u}_s\|$. The assumption of infinitesimal deformations requires that $\epsilon \ll 1$. We develop the well-known linear theory by retaining terms to first order in ϵ , neglecting terms of order ϵ^2 and higher. Note that the deformation itself enters at first order by definition.

A. Linear flow equation

We have from Equations (3) and (4) that

$$\frac{\phi_f - \phi_{f,0}}{1 - \phi_{f,0}} \approx \nabla \cdot \mathbf{u}_s \sim \epsilon. \quad (21)$$

This motivates rewriting Equation (14a) in terms of the normalized change in porosity, $\tilde{\phi}_f \equiv (\phi_f - \phi_{f,0})/(1 - \phi_{f,0}) \sim \epsilon$,

$$\frac{\partial \tilde{\phi}_f}{\partial t} + \nabla \cdot \left[\tilde{\phi}_f \mathbf{q} - (1 - \tilde{\phi}_f) \frac{k(\phi_f)}{\mu} (\nabla p - \rho_f \mathbf{g}) \right] = 0, \quad (22)$$

where we have taken the initial porosity field to be uniform. We then eliminate \mathbf{q} in favor of \mathbf{v}_s using Equation (15b),

$$\frac{\partial \tilde{\phi}_f}{\partial t} + \nabla \cdot \left[\tilde{\phi}_f \mathbf{v}_s - \frac{k(\phi_f)}{\mu} (\nabla p - \rho_f \mathbf{g}) \right] = 0. \quad (23)$$

Equation (7) implies that $\|\mathbf{v}_s\| \sim \delta$, and therefore that $\|\nabla \cdot (\tilde{\phi}_f \mathbf{v}_s)\| \sim \epsilon^2$. Simplifying Equation (23) accordingly, we arrive at one form of the well-known linear poroelastic flow equation:

$$\frac{\partial \phi_f}{\partial t} - \nabla \cdot \left[(1 - \phi_{f,0}) \frac{k_0}{\mu} (\nabla p - \rho_f \mathbf{g}) \right] \approx 0, \quad (24)$$

where $k_0 = k(\phi_{f,0})$ is the relaxed/undeformed permeability, and where we have reverted from $\tilde{\phi}_f$ to ϕ_f .

Comparing Equation (24) with Equations (14) highlights the fact that exact kinematics not only render the model nonlinear, but also introduce a fundamentally different mathematical character: Equation (24) can be written as a linear diffusion equation after introducing linear elasticity in the solid skeleton, whereas Equations (14) feature an additional, advection-like term related to the divergence-free total flux.

B. Linear elasticity

It is straightforward to show that Hencky elasticity (§II H) reduces to classical linear elasticity at leading order in ϵ , as do many other (but not all) finite-deformation elasticity laws. Linear elasticity can be written as

$$\boldsymbol{\sigma}' = \Lambda \text{tr}(\boldsymbol{\varepsilon}) \mathbf{I} + (\mathcal{M} - \Lambda) \boldsymbol{\varepsilon}, \quad \text{and} \quad (25a)$$

$$\boldsymbol{\varepsilon} = \frac{1}{2} [\nabla \mathbf{u}_s + (\nabla \mathbf{u}_s)^\top], \quad (25b)$$

where $\boldsymbol{\varepsilon}$ is the infinitesimal (“small”) strain tensor. By linearizing the strain in the displacement ($\mathbf{H} \approx \boldsymbol{\varepsilon}$) and the stress in the strain ($J\boldsymbol{\sigma}' \approx \boldsymbol{\sigma}'$), linear elasticity neglects both kinematic nonlinearity and constitutive nonlinearity, and also the distinction between the deformed configuration and the reference configuration.

C. Discussion

A closed linear theory is provided by combining the linear flow equation (Eq. 24) with mechanical equilibrium (Eq. 19), linear elasticity (Eqs. 25), and the linearized statement of volumetric compatibility (Eq. 21). The resulting model is valid to first order in ϵ . A discussion of the various forms of the linear theory commonly used in hydrology, hydrogeology, and petroleum engineering can be found in Ref. [17], and reviews of numerous classical results in linear poroelasticity can be found in Refs. [17] and [30].

Note that variations in permeability do not enter at this order because Equations (19) and (25) together imply that $\|\nabla p/(\mathcal{M}/\mathcal{L})\| = \|(\nabla \cdot \boldsymbol{\sigma}')/(\mathcal{M}/\mathcal{L})\| \sim \epsilon$. This latter scaling should also be viewed as a constraint: Imposing pressure or stress gradients of size approaching \mathcal{M}/\mathcal{L} will drive a deformation that violates the assumption $\epsilon \ll 1$, invalidating the linear theory.

The linear theory can alternatively be derived from a Lagrangian perspective (Ref. [32] and Appendix A). This must necessarily result in the same model, but in terms of the Lagrangian coordinate \mathbf{X} instead of the Eulerian coordinate \mathbf{x} . These coordinates themselves differ at first order, $\|(\mathbf{x} - \mathbf{X})/\mathcal{L}\| = \|\mathbf{u}_s/\mathcal{L}\| \sim \epsilon$, but all quantities related to the deformation are also first order and this implies, for example, that $p(\mathbf{X}, t) = p(\mathbf{x}, t) - (\nabla p) \cdot \mathbf{u}_s + \dots \approx p(\mathbf{x}, t)$. As a result, replacing \mathbf{x} with \mathbf{X} in Equations (19), (21), (24), and (25) will result in a Lagrangian interpretation of the linear model that is still valid to first order in ϵ . These two models are equivalent in the limit of $\epsilon \rightarrow 0$, but they will always differ at order ϵ^2 and diverge from each other as the deformation grows. This conceptual ambiguity is one awkward aspect of linear (poro)elasticity (see also, Appendix B).

Here, our interest is in the behavior of the linear theory as the deformation becomes non-negligible. We next consider two model problems involving uniaxial flow and deformation, using these as a convenient setting for com-

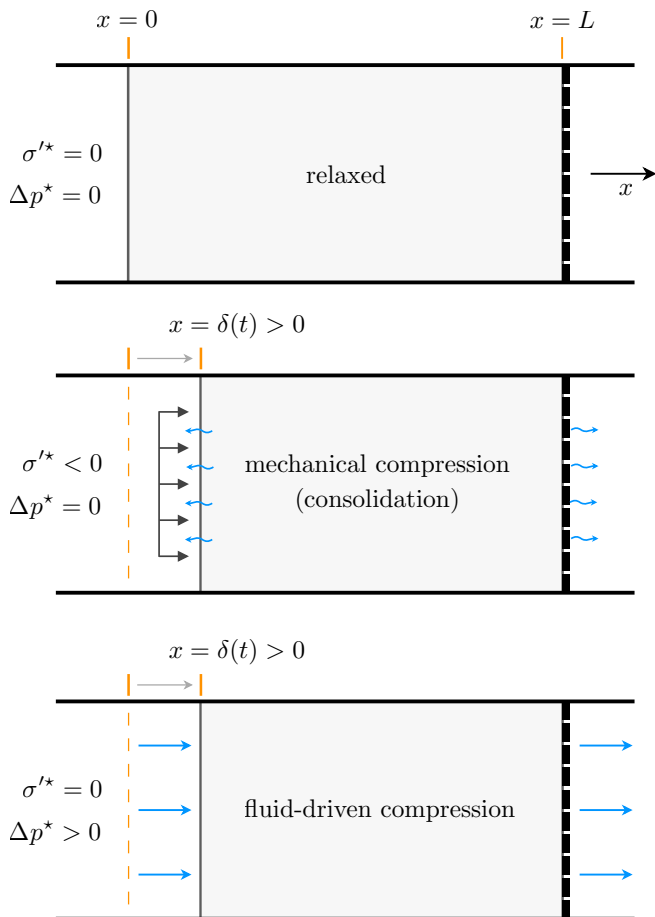


FIG. 1. We consider the uniaxial deformation of a soft porous material by an applied effective stress and/or an applied fluid pressure drop. (a) The solid is laterally confined and has relaxed length L . Its right edge is attached to a rigid permeable barrier ($x = L$, thick dashed black line), but the rest is free to move. We denote the instantaneous position of the left edge by $x = \delta(t)$, taking $\delta(0) = 0$ (dashed orange line). The material can be compressed against the barrier ($\delta > 0$) by (b) an applied effective stress $\sigma'^* < 0$ (dark gray arrows), in which case the rate of deformation is set by the rate of fluid outflow (wiggly blue arrows) and/or by (c) an applied fluid pressure drop $\Delta p^* > 0$, in which case the deformation is driven by a net flow from left to right (straight blue arrows).

paring the predictions of linear poroelasticity with the large-deformation theory.

IV. MODELS FOR UNIAXIAL FLOW AND DEFORMATION

We now consider the uniaxial deformation of a deformable porous material, as shown schematically in Figure 1. Provided that the material properties are uniform in the lateral directions, both the flow and the deforma-

tion will be restricted to one spatial dimension,

$$\mathbf{v}_f = v_f(x, t)\hat{e}_x, \quad (26a)$$

$$\mathbf{v}_s = v_s(x, t)\hat{e}_x, \quad (26b)$$

$$\mathbf{u}_s = u_s(x, t)\hat{e}_x, \quad (26c)$$

and

$$\phi_f = \phi_f(x, t). \quad (26d)$$

As a result, the analysis is tractable even when the deformation is large. This allows for the exploration of a variety of complex material models [68–70] and loading scenarios, including mechanical compression [71, 72], forced infiltration [70, 73], and spontaneous imbibition [74, 75]. Here, we consider two canonical problems: Mechanical compression (the consolidation problem) and fluid-driven compression. These differ only in the boundary conditions, so we develop a single model that applies to both cases. We assume that gravity is unimportant.

For the solid, a one-dimensional displacement field implies that the material is either laterally confined or laterally infinite, otherwise the Poisson effect would lead to lateral expansion or contraction. Our model and results are independent of the shape and size of the y - z cross-section as long as the lateral boundaries are rigid, frictionless, and impermeable. For example, the material could be a rectangular slab within a duct [e.g., 76, 77] or a cylinder within a tube [e.g., 78]. Although we focus here on compression, our models and solutions remain valid if we reverse the sign of the effective stress and/or the pressure gradient; this will reverse the direction of the displacement and/or the flow, stretching the skeleton to the left in a state of tension.

A. Five models

Poromechanical phenomena are highly coupled. In order to highlight the nonlinear interactions between the various physical mechanisms at play, as well the qualitative and quantitative behavior of the error introduced by linearizing these, we consider five different models below: A fully linear model (§III), two fully nonlinear models, and two intermediate models. The nonlinear models combine rigorous large-deformation kinematics with Hencky elasticity (§II H) and one of two permeability laws: Constant ($k = k_0$) or deformation-dependent ($k = k(\phi_f)$) via the normalized Kozeny-Carman formula, Eq. (12). The intermediate models are the same as the nonlinear models, but replacing Hencky elasticity with linear elasticity (§III B) while retaining all other nonlinearity. We refer to these models as:

1. “linear”: Linear poroelasticity;
2. “nonlinear- k_0 ”: Nonlinear kinematics with Hencky elasticity and constant permeability;

3. “nonlinear- k_{KC} ”: Nonlinear kinematics with Hencky elasticity and deformation-dependent permeability;
4. “intermediate- k_0 ”: Nonlinear kinematics with linear elasticity and constant permeability; and
5. “intermediate- k_{KC} ”: Nonlinear kinematics with linear elasticity and deformation-dependent permeability.

Note that although the intermediate approach is nonlinear, and retains most of the kinematic nonlinearity of the fully nonlinear model, it is not kinematically rigorous because the nonlinearity of Hencky elasticity is also kinematic in origin. The intermediate approach should also be considered with caution because it is asymptotically mixed, which can lead to non-physical behavior at large deformations. However, it is useful for illustration.

We derive and discuss below the fully nonlinear models (§IV B) and the linear model (§IV C), but we present results from all five models [79]. We adopt the shorthand names given above for conciseness.

B. Large-deformation poroelasticity

We first consider the exact kinematics of flow and deformation with a Hencky-elastic response in the solid skeleton. The results from this section provide the nonlinear- k_0 and nonlinear- k_{KC} models by introducing the appropriate permeability function, and can be readily modified to provide the intermediate- k_0 and intermediate- k_{KC} models by replacing Hencky elasticity with linear elasticity in any steps involving the elasticity law.

1. Kinematics and flow

We assume that the porosity in the initial state is spatially uniform and given by $\phi_f(x, 0) = \phi_{f,0}$, where $\phi_{f,0}$ is a known constant, thereby giving

$$J(x, t) = \frac{1 - \phi_{f,0}}{1 - \phi_f(x, t)}. \quad (27)$$

The deformation-gradient tensor can be written as (*c.f.*, Equation 3)

$$\mathbf{F} = \begin{bmatrix} J & 0 & 0 \\ 0 & 1 & 0 \\ 0 & 0 & 1 \end{bmatrix}, \quad (28)$$

where the Jacobian determinant is

$$J = \det(\mathbf{F}) = \left(1 - \frac{\partial u_s}{\partial x}\right)^{-1}. \quad (29)$$

The displacement field is linked to the porosity field via Equation (27),

$$\frac{\phi_f - \phi_{f,0}}{1 - \phi_{f,0}} = \frac{\partial u_s}{\partial x}. \quad (30)$$

For uniaxial flow, Equations (14), (15), and (19) become

$$\frac{\partial \phi_f}{\partial t} + \frac{\partial}{\partial x} \left[\phi_f q(t) - (1 - \phi_f) \frac{k(\phi_f)}{\mu} \frac{\partial p}{\partial x} \right] = 0, \quad (31a)$$

with

$$v_f = q(t) - \left(\frac{1 - \phi_f}{\phi_f} \right) \frac{k(\phi_f)}{\mu} \frac{\partial p}{\partial x}, \quad (31b)$$

$$v_s = q(t) + \frac{k(\phi_f)}{\mu} \frac{\partial p}{\partial x}, \quad (31c)$$

and

$$\frac{\partial p}{\partial x} = \frac{\partial \sigma'_{xx}}{\partial x}, \quad (31d)$$

where the total volume flux $q(t) = \phi_f v_f + (1 - \phi_f) v_s$ is a function of time only. Equations (30) and (31) constitute a kinematically exact model for any constitutive behavior in the solid skeleton. This model has been derived previously [*e.g.*, Equation (44) of Ref. 70].

2. Hencky elasticity

We take the constitutive response of the solid skeleton to be Hencky elastic, in which case the associated effective stress is

$$\boldsymbol{\sigma}' = \begin{bmatrix} \mathcal{M} \frac{\ln J}{J} & 0 & 0 \\ 0 & \Lambda \frac{\ln J}{J} & 0 \\ 0 & 0 & \Lambda \frac{\ln J}{J} \end{bmatrix}. \quad (32)$$

Although the displacement and the strain are uniaxial, the stress has three nontrivial components due to the Poisson effect under lateral confinement. If the material were laterally unconfined, the stress would be uniaxial and the strain would have three nontrivial components.

We link the mechanics of the skeleton with those of the fluid by combining Equation (32) with Equations (30) and (31d) to obtain

$$\begin{aligned} \frac{\partial p}{\partial x} &= \frac{\partial \sigma'_{xx}}{\partial x} = \frac{\partial}{\partial x} \left[\mathcal{M} \frac{\ln J}{J} \right] \\ &= \frac{\partial}{\partial x} \left[\mathcal{M} \left(\frac{1 - \phi_f}{1 - \phi_{f,0}} \right) \ln \left(\frac{1 - \phi_{f,0}}{1 - \phi_f} \right) \right]. \end{aligned} \quad (33)$$

With appropriate boundary conditions, Equations (30)–(33) finally provide a closed model for the evolution of the porosity.

For uniaxial deformation, the Hencky stress and strain depend only on J and can therefore be written directly in terms of ϕ_f . In fact, this is the case for any constitutive law since \mathbf{F} itself depends only on J —that is, the deformation can be completely characterized by the local change in porosity. This is a special feature of uniaxial deformation: The effective stress can be written exclusively as a function of porosity, $\boldsymbol{\sigma}' = \boldsymbol{\sigma}'(\phi_f)$, for any constitutive law. As a result, the framework of large-deformation elasticity can be avoided in a uniaxial setting by simply positing or measuring the function $\sigma'_{xx}(\phi_f)$ [e.g., 80]. This approach is simple and appealing, but has the obvious disadvantage that it cannot be readily generalized to more complicated loading scenarios. It also has the more subtle disadvantage that even in the uniaxial case it is unable to provide answers to basic questions about the 3D state of stress within the material. For example: How much stress does the material apply to the lateral confining walls? What is the maximum shear stress within the material?

3. Boundary conditions

The left and right boundaries of the solid skeleton are located at $x = \delta(t)$ and $x = L$, respectively, and we take $\delta(0) = 0$ without loss of generality (Figure 1). We then have four kinematic boundary conditions for the skeleton from the fact that the left and right edges are material boundaries: Two on displacement,

$$u_s(\delta, t) = \delta \quad \text{and} \quad u_s(L, t) = 0, \quad (34)$$

and two on velocity,

$$v_s(\delta, t) = \dot{\delta} \equiv \frac{d\delta}{dt} \quad \text{and} \quad v_s(L, t) = 0. \quad (35)$$

We use the former pair in calculating the displacement field from the porosity field, and the latter pair in deriving boundary conditions for porosity.

We take the pressure drop across the material to be imposed and equal to $\Delta p \equiv p(\delta, t) - p(L, t)$, and without loss of generality we write this as

$$p(\delta, t) = \Delta p \quad \text{and} \quad p(L, t) = 0. \quad (36)$$

We further assume that a mechanical load is applied to the left edge in the form of an imposed effective stress σ'^* . The effective stress at the right edge can then be derived by integrating Equation (31d) from δ to L to arrive at $\sigma_{xx}(\delta, t) = \sigma_{xx}(L, t)$, which is simply a statement of macroscopic force balance in the absence of inertia or body forces. From this and the pressures at δ and L , we then have that

$$\sigma'_{xx}(\delta, t) = \sigma'^* \quad \text{and} \quad \sigma'_{xx}(L, t) = \sigma'^* - \Delta p. \quad (37)$$

Since the effective stress is directly related to the porosity in this geometry (see §IV B 2), Equations (37) pro-

vide $\phi_f(\delta, t)$ and $\phi_f(L, t)$ and constitute Dirichlet conditions. For Hencky elasticity, these can be readily calculated from

$$\phi_f(x, t) = 1 + (1 - \phi_{f,0}) \frac{\sigma'_{xx}/\mathcal{M}}{W(-\sigma'_{xx}/\mathcal{M})} \quad (38)$$

where $W(\cdot)$ denotes the Lambert W function ($y = W(x)/x$ solves $x = -\ln(y)/y$).

When the pressure drop is imposed, the volume flux $q(t)$ through the material will vary in time and this appears explicitly in Equations (31). One approach to deriving an expression for $q(t)$ is to rearrange and integrate Equation (31c) [c.f., Equations (21)–(23) of 70],

$$q(t) = \frac{\Delta p^* + \int_{\delta}^L \frac{\mu}{k(\phi_f)} v_s dx}{\int_{\delta}^L \frac{\mu}{k(\phi_f)} dx}, \quad (39)$$

but this is awkward in practice since it requires explicit calculation of v_s from u_s via Equation (7), which is otherwise unnecessary. Alternatively, we can evaluate Equation (31c) at $x = L$ to obtain

$$q(t) = - \left[\frac{k(\phi_f)}{\mu} \frac{\partial p}{\partial x} \right] \Big|_{x=L} = - \left[\frac{k(\phi_f)}{\mu} \frac{d\sigma'_{xx}}{d\phi_f} \frac{\partial \phi_f}{\partial x} \right] \Big|_{x=L}, \quad (40)$$

which we supplement with the Dirichlet condition above on $\phi_f(L, t)$. Equation (40) is straightforward to implement.

For fluid-driven deformation, an imposed pressure drop Δp^* will eventually lead to a steady state in which the solid is stationary, the fluid flow is steady, and the volume flux is constant, $q(t) \rightarrow q^*$. Imposing instead this same flux q^* from the outset and allowing the pressure drop to vary must eventually lead to precisely the same steady state, in which $\Delta p(t) \rightarrow \Delta p^*$. As a result, the only difference between these two conditions is in the dynamic approach to steady state. We focus on the pressure-driven case below, but we provide analytical and numerical solutions that are valid for both cases [79] and we explore the relationship between q^* and Δp^* at steady state. Note that, for an imposed flux, the pressure at $x = \delta$ is unknown and the Dirichlet condition at $x = L$ must be replaced by the Neumann condition that $\phi_f(L, t)v_f(L, t) = q^*$.

For an incompressible solid skeleton, conservation of solid volume requires that

$$\int_{\delta}^L (1 - \phi_f) dx = (1 - \phi_{f,0}) L, \quad (41)$$

and it is straightforward to confirm that this is identically satisfied by Equations (30) and (34). If any of these relationships are approximated, the resulting model will no longer be volume-conservative. Conservation of mass or volume is typically not a primary concern in solid mechanics because most engineering materials are only

slightly compressible and typically experience very small deformations. It becomes more important in poromechanics because porous materials are much more compressible than non-porous ones since the skeleton can deform through rearrangement of the solid grains. This allows for large volume changes through large changes in the pore volume, which are then strongly coupled to the fluid mechanics.

C. Linear poroelasticity

We now derive the linear model. We do this by linearizing the nonlinear model above, so we write the results in terms of the Eulerian coordinate x . As described in §III C, however, the spatial coordinate in the linear model is ambiguous: Simply replacing the Eulerian coordinate x with the Lagrangian coordinate X in the expressions below will result in a model that is still accurate to leading order in δ/L . Whereas the Eulerian interpretation of this model (with x) will only satisfy the boundary conditions at $x = \delta$ at first order, the resulting Lagrangian interpretation (with X) will satisfy them exactly at $X = 0$. However, the Eulerian interpretation will respect the relationship between porosity and displacement exactly since this is linear in the Eulerian coordinate (*c.f.*, Equation 42), whereas the Lagrangian interpretation will respect this only at first order.

1. Kinematics and flow

Adopting the assumption of infinitesimal deformations and linearizing in the strain, Equation (21) becomes

$$\frac{\phi_f - \phi_{f,0}}{1 - \phi_{f,0}} = \frac{\partial u_s}{\partial x}. \quad (42)$$

Note that this is identical to Equation (30), and is therefore exact. This is another special feature of uniaxial deformation: The exact relationship between ϕ_f and u_s is linear. This does not hold for even simple biaxial deformations.

From Equations (19) and (24), we further have

$$\frac{\partial \phi_f}{\partial t} - \frac{\partial}{\partial x} \left[(1 - \phi_{f,0}) \frac{k_0}{\mu} \frac{\partial p}{\partial x} \right] \approx 0, \quad (43a)$$

$$\frac{\partial p}{\partial x} = \frac{\partial \sigma'_{xx}}{\partial x}. \quad (43b)$$

Comparing Equation (43a) with Equation (31a) again highlights the fundamentally different mathematical character of the linear model as compared to the nonlinear model.

2. Linear elasticity

We take the constitutive response of the solid skeleton to be linear elastic, in which case the associated effective

stress tensor is

$$\boldsymbol{\sigma}' = \begin{bmatrix} \mathcal{M} \frac{\partial u_s}{\partial x} & 0 & 0 \\ 0 & \Lambda \frac{\partial u_s}{\partial x} & 0 \\ 0 & 0 & \Lambda \frac{\partial u_s}{\partial x} \end{bmatrix}. \quad (44)$$

Combining this with Equations (42) and (43b), we obtain

$$\frac{\partial p}{\partial x} = \frac{\partial \sigma'_{xx}}{\partial x} = \frac{\partial}{\partial x} \left[\mathcal{M} \frac{\partial u_s}{\partial x} \right] = \frac{\partial}{\partial x} \left[\mathcal{M} \left(\frac{\phi_f - \phi_{f,0}}{1 - \phi_{f,0}} \right) \right]. \quad (45)$$

With appropriate boundary conditions, Equations (42)–(45) provide a closed linear model for the evolution of the porosity.

3. Boundary conditions

The kinematic conditions on the solid displacement (Eqs. 34) become

$$u_s(0, t) \approx \delta \quad \text{and} \quad u_s(L, t) = 0, \quad (46)$$

where the distinction between $u_s(\delta, t)$ and $u_s(0, t)$ does not enter at first order. The latter condition is used when calculating the displacement field from the porosity field, and the former then provides an expression for $\delta(t)$. Neither is necessary when solving for the porosity field itself.

For an imposed pressure drop, the dynamic conditions on the pressure and the stress become

$$\sigma'_{xx}(0, t) \approx \sigma'^* \quad \text{and} \quad \sigma'_{xx}(L, t) = \sigma'^* - \Delta p^*, \quad (47)$$

and these again provide Dirichlet conditions on the porosity via the elasticity law,

$$\phi_f(x, t) = \phi_{f,0} + (1 - \phi_{f,0}) \frac{\sigma'_{xx}}{\mathcal{M}}. \quad (48)$$

With these conditions on porosity, the linear model is fully specified. It is not necessary to calculate the total flux because it does not appear explicitly in the linear conservation law, but the flux can be calculated at any time from

$$v_s(L, t) = 0 \quad \rightarrow \quad q(t) \approx - \frac{1}{(1 - \phi_{f,0})} \frac{k_0 \mathcal{M}}{\mu} \frac{\partial \phi_f}{\partial x} \Big|_{x=L}. \quad (49)$$

When the flux is imposed instead of the pressure drop, Equation (49) can be rearranged to provide a Neumann condition at $x = L$ that replaces the Dirichlet condition above. The pressure drop $\Delta p(t)$ is then unknown, and must be calculated by rearranging Equations (47) and (48).

D. Scaling

We consider the natural scaling

$$\begin{aligned} \tilde{t} &= \frac{t}{T_{\text{pe}}}, & \tilde{x} &= \frac{x}{L}, & \tilde{k} &= \frac{k}{k_0}, \\ \tilde{p} &= \frac{p}{\mathcal{M}}, & \tilde{\sigma}'_{xx} &= \frac{\sigma'_{xx}}{\mathcal{M}}, & \tilde{u}_s &= \frac{u_s}{L}, \end{aligned} \quad (50)$$

where the characteristic permeability is $k_0 = k(\phi_{f,0})$ and the classical poroelastic timescale is $T_{\text{pe}} = \mu L^2 / (k_0 \mathcal{M})$. The problem is then controlled by one of two dimensionless groups that measure the strength of the driving stresses relative to the stiffness of the skeleton: $\tilde{\sigma}'^* \equiv \sigma'^* / \mathcal{M}$ for deformation driven by an applied mechanical load, or $\Delta \tilde{p}^* \equiv \Delta p^* / \mathcal{M}$ for deformation driven by fluid flow with a constant pressure drop Δp^* . For an imposed flux q^* , the relevant dimensionless group is instead $\tilde{q}^* \equiv \mu q^* L / (k_0 \mathcal{M})$.

The problem also depends on the initial porosity $\phi_{f,0}$. When the permeability is constant, $\phi_{f,0}$ can be scaled out by working instead with the normalized change in porosity,

$$\tilde{\phi}_f = \frac{\phi_f - \phi_{f,0}}{1 - \phi_{f,0}}. \quad (51)$$

When the permeability is allowed to vary, the initial value $\phi_{f,0}$ cannot be eliminated because the permeability must depend on the current porosity rather than on the change in porosity.

The discussion below uses dimensional quantities for expository clarity, but we present the results in terms of dimensionless parameter combinations to emphasize this scaling.

E. Summary

Each of the models described above can ultimately be written as a single parabolic conservation law for ϕ_f ; this will be linear and diffusive for the linear model, and nonlinear and advective-diffusive for the intermediate and nonlinear models. The boundary condition at the left is a Dirichlet condition for all of the cases considered here, and the boundary condition at the right is either Dirichlet for flow driven by a imposed pressure drop or Neumann for flow driven by an imposed fluid flux. For the nonlinear and intermediate models, we must also solve for the unknown position of the free left boundary. Below, we study these models dynamically and at steady-state in the context of two model problems.

V. MECHANICAL COMPRESSION: THE CONSOLIDATION PROBLEM

We now consider the uniaxial mechanical compression of a porous material (Figure 1b), in which an effective stress σ'^* is suddenly applied to the left edge of

the material at $t = 0^+$ and the fluid pressure at both edges is held constant and equal to the ambient pressure, $p(\delta, t) = p(L, t) = 0$. The process by which the material relaxes under this load, squeezing out fluid as the pore volume decreases, is known as *consolidation*. The consolidation problem is a classical one, with direct application to the engineering of foundations; it has been studied extensively in that context and others [e.g., 5, 17, 40, 51, 81–83].

Force balance requires that the total stress everywhere in the material must immediately support the applied load, $\sigma_{xx}(x, t) = \sigma'_{xx}(x, t) - p(x, t) = \sigma'^*$ for $t > 0$. However, the effective stress can only contribute through strain in the solid skeleton, and the solid skeleton can only deform by displacing fluid, and this is not instantaneous. As a result, the fluid pressure must immediately jump to support the entire load: $p(x, 0^+) = -\sigma'^*$. In soil and rock mechanics, this is known as an *undrained* response: The mechanical response of a fluid-solid mixture under conditions where the fluid content is fixed. Over time, this high pressure relaxes as fluid flows out at the boundaries, and the effective stress supports an increasing fraction of the load as the material is compressed. When the process is finished, the effective stress will support the entire load and the fluid pressure will have returned to its ambient value. This is classical consolidation theory.

A. Steady state

When the consolidation process is finished, the solid and fluid are both stationary, $v_s(x) = v_f(x) = 0$, and the fluid pressure is uniform, $p(x) = 0$. As a result, the steady state is determined entirely by the boundary conditions and the elastic response of the skeleton; the fluid plays no role. In soil and rock mechanics, this is known as the *drained* response of the material.

Without a fluid pressure gradient, mechanical equilibrium implies that the effective stress and therefore also the porosity must be uniform, $\sigma'_{xx}(x) = \sigma'^*$ and $\phi_f(x) = \phi_f^*$ (Eqs. 33 and 45). Since the fluid plays no role, the nonlinear- k_0 and nonlinear- k_{KC} models are identical in steady-state. For both of these, we have that

$$\frac{\phi_f^* - \phi_{f,0}}{1 - \phi_{f,0}} = 1 - \frac{1}{J^*}, \quad (52a)$$

$$\frac{u_s(x)}{L} = - \left(1 - \frac{1}{J^*} \right) \left(1 - \frac{x}{L} \right), \quad (52b)$$

$$\frac{\delta^*}{L} = 1 - J^*, \quad (52c)$$

where the Jacobian determinant J^* is found by inverting $\sigma'_{xx}(J^*) = \sigma'^*$ with the aid of Equation 38,

$$J^* = - \frac{W(-\sigma'^* / \mathcal{M})}{\sigma'^* / \mathcal{M}}, \quad (53)$$

and the deflection δ^*/L is the change in length per unit reference length, usually known as the “engineering” or *nominal* strain. For the linear model, we instead have that

$$\frac{\phi_f^* - \phi_{f,0}}{1 - \phi_{f,0}} \approx \frac{\sigma'^*}{\mathcal{M}}, \quad (54a)$$

$$\frac{u_s(x)}{L} \approx -\frac{\sigma'^*}{\mathcal{M}} \left(1 - \frac{x}{L}\right), \quad \text{and} \quad (54b)$$

$$\frac{\delta^*}{L} \approx -\frac{\sigma'^*}{\mathcal{M}}. \quad (54c)$$

We compare these results in Figure 2, showing the linear model (Lagrangian interpretation), the nonlinear- k_0 model, and the nonlinear- k_{KC} model (see §IV A). We include the latter for completeness but, as mentioned above, it is identical to the nonlinear- k_0 model at steady state since there is no flow.

In all cases, the only nontrivial component of the deformation is the displacement, and this is simply linear in x . The difference between the models lies in the amount of deformation that results from a given load: The nonlinear and intermediate models deform much less than the linear model, and increasingly so for larger compressive loads (Figure 3). The relative error between the linear and nonlinear models is $\sim \delta^*/L$, which is consistent with the assumptions of linear (poro)elasticity. To highlight the origin of this error, we further compare these two models with the intermediate model, in which we replace Hencky elasticity with linear elasticity in the nonlinear kinematic framework (see §IV A; Figure 3). This comparison illustrates the fact that the majority of the error associated with the linear model results in this case from the kinematics of the deformation, and not from nonlinearity in the elasticity law. One source of kinematic nonlinearity at steady state is the cumulative nature of strain, where increments of displacement correspond to

increasingly larger increments of strain as the material is compressed because the overall length decreases. The opposite occurs in tension: The nonlinear model deforms much more than the linear model because increments of displacement correspond to increasingly smaller increments of strain as the material is stretched. Another source of kinematic nonlinearity is the moving boundary, since the linear model only satisfies the boundary conditions there at leading order in δ^*/L .

The nonlinear model implies that the material can support an arbitrarily large compressive stress, with δ^*/L approaching unity (*i.e.*, the length of the deformed solid approaching zero) as the compressive stress diverges. Closer inspection reveals that the porosity will vanish when the deflection δ^*/L reaches $\phi_{f,0}$, which occurs at a finite compressive stress. One would expect the stiffness of the skeleton to change relatively sharply across the transition from compressing pore space to compressing solid grains, and significant microstructural damage would likely occur *en route* (*e.g.*, grain crushing)—A material-specific constitutive model would be necessary to capture this. This behavior is also important and problematic from the perspective of the fluid mechanics, which can become non-physical unless the permeability law accounts appropriately for the changing porosity (see §II E above).

B. Dynamics

To explore the dynamics of consolidation, we solve the nonlinear and intermediate models numerically using a finite-volume method with an adaptive grid (Appendix C and [79]), and we solve the linear model analytically via separation of variables. The well-known analytical solution can be written

$$\phi_f(x, t) = \phi_f^* - (\phi_f^* - \phi_{f,0}) \sum_{n=1}^{\infty} \frac{2}{n\pi} \left[1 + (-1)^{n+1}\right] e^{-\frac{(n\pi)^2 t}{T_{pe}}} \sin\left(\frac{n\pi x}{L}\right) \quad \text{and} \quad (55a)$$

$$\frac{u_s(x, t)}{L} = -\left(\frac{\phi_f^* - \phi_{f,0}}{1 - \phi_{f,0}}\right) \left\{1 - \frac{x}{L} + \sum_{n=1}^{\infty} \frac{2}{(n\pi)^2} \left[1 + (-1)^{n+1}\right] e^{-\frac{(n\pi)^2 t}{T_{pe}}} \left[(-1)^n - \cos\left(\frac{n\pi x}{L}\right)\right]\right\}, \quad (55b)$$

where $\phi_f(0, t) = \phi_f(L, t) = \phi_f^* = \phi_{f,0} + (1 - \phi_{f,0})(\sigma'^*/\mathcal{M})$, as in Equation (54a), and all other quantities of interest can readily be calculated from the porosity and displacement fields. Note that, as in the steady state, the Eulerian interpretation of Equations (55) (as written) only satisfies the boundary conditions at the moving boundary to leading order in δ^*/L . The Lagrangian interpretation (replacing x with X) rigorously satisfies the boundary conditions at $X = 0$, but at the ex-

pense of exact conservation of mass (Eq. 42). However, both interpretations predict the same deflection, which is often the quantity of primary interest in engineering applications (Eulerian: $\delta^* \approx u_s(x = 0, t)$; Lagrangian: $\delta^* = u_s(X = 0, t)$).

In Figure 4, we compare the dynamics of consolidation for the linear model (Lagrangian interpretation), the nonlinear- k_0 model, and the nonlinear- k_{KC} model. In all cases, the skeleton is initially relaxed in the middle

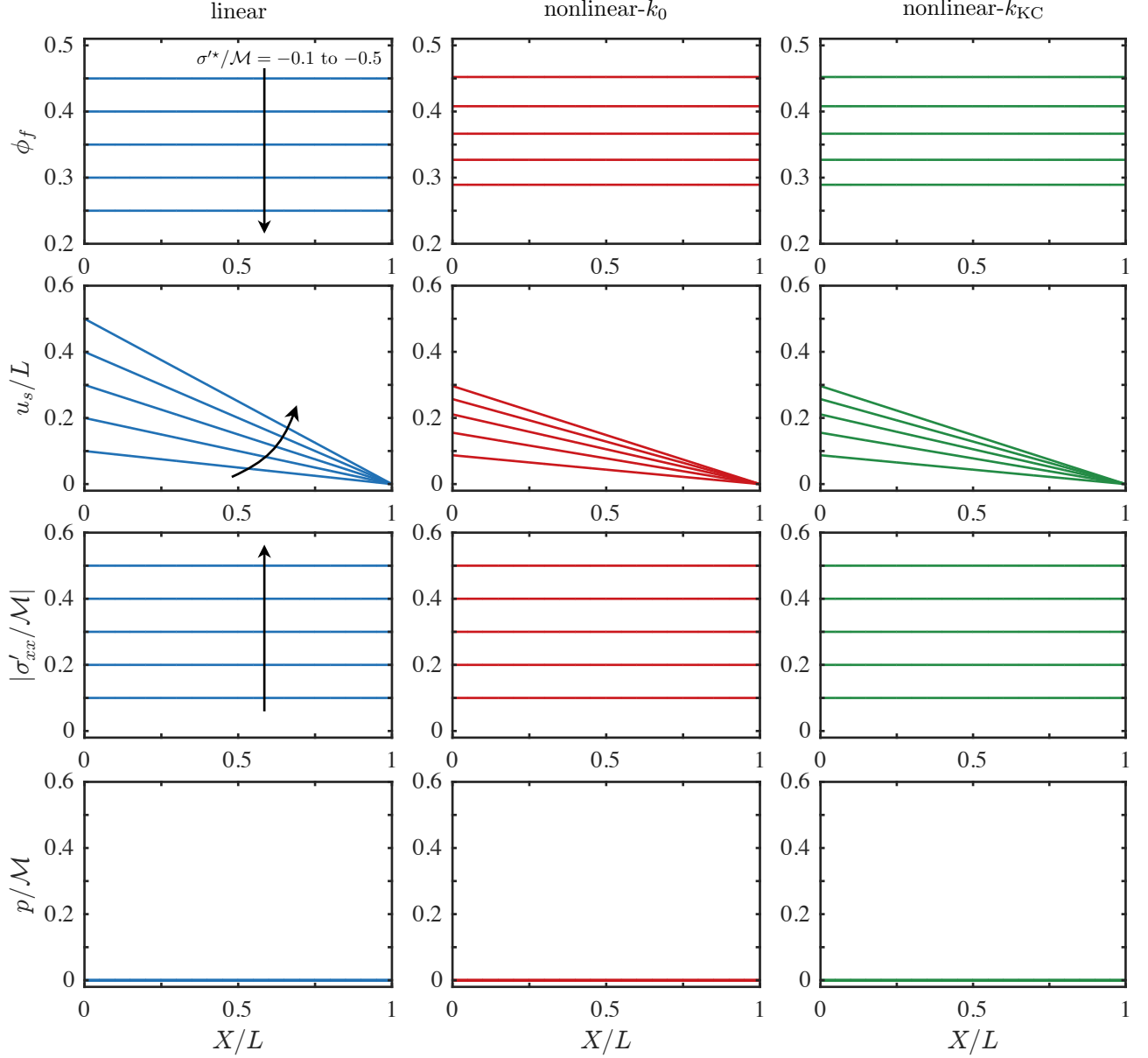


FIG. 2. Steady state in the consolidation of a soft porous material under an applied effective stress $\sigma'^* < 0$, here for $\sigma'^*/\mathcal{M} = -0.1, -0.2, -0.3, -0.4$, and -0.5 , as indicated. We show the porosity (taking $\phi_{f,0} = 0.5$; first row), displacement (second row), effective stress (third row), and pressure (last row) for the linear model (left column, blue), the nonlinear- k_0 model (middle column, red), and the nonlinear- k_{KC} model (right column, green) (see §IV A). For the nonlinear models, we plot these results against the Lagrangian coordinate $X = x - u_s(x, t)$ for clarity; for the linear model, we adopt a Lagrangian interpretation and simply replace x with X in the relevant expressions (see §III C and §V B). In all cases, the displacement is linear and the porosity, stress, and pressure are uniform. Fluid flow plays no role in the steady state, so the middle and right columns are identical.

and very strongly deformed at the edges, from which the fluid can easily escape. The deformation propagates inward toward the middle from both ends over time, and the pressure decays as the skeleton supports an increasing fraction of the total stress. The nonlinear- k_{KC} model

exhibits a more rounded deformation profile than either the linear model or the nonlinear- k_0 model, which is a result of the fact that the reduced permeability in the compressed outer regions slows and spreads the relaxation of the pressure field. The two nonlinear models

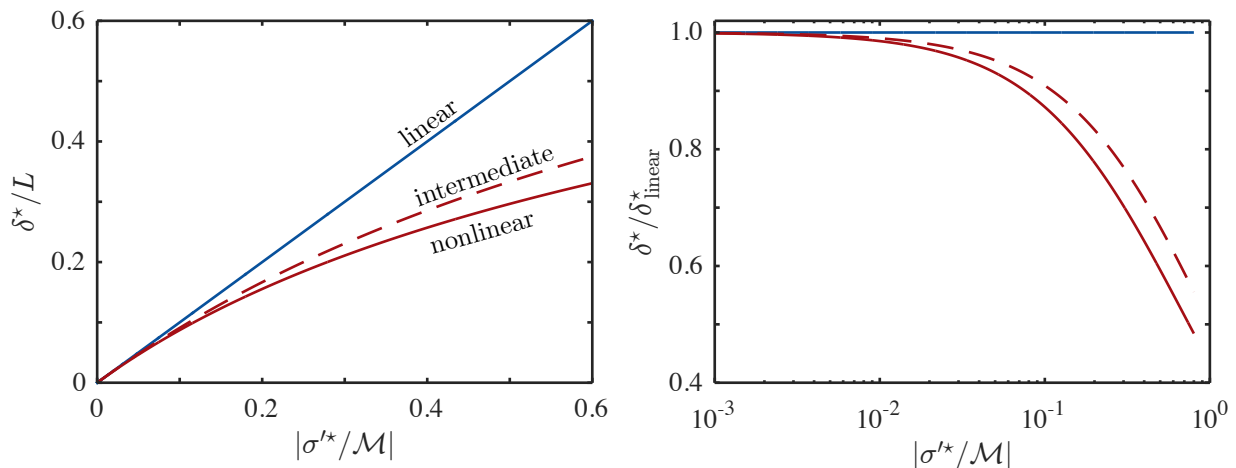


FIG. 3. The linear model over-predicts the final deflection in consolidation under an applied effective stress, and this error is primarily kinematic. Here we plot (a) the final deflection δ^*/L against the applied effective stress σ^*/\mathcal{M} for the linear model (blue), the nonlinear model (solid red), and the intermediate model (dashed red) (see §IV A). We also show (b) the ratio of these predictions to the linear one, $\delta^*/\delta_{\text{linear}}^*$, on a semilogarithmic scale. The nonlinear and intermediate models both exhibit much stiffer behavior than the linear model in compression, and the nonlinear model is stiffer than the intermediate model. The relative error in both the linear and intermediate models is $\sim\delta^*/L$, which is consistent with the assumptions of linear (poro)elasticity.

ultimately arrive at the same steady state, which is determined strictly by the elasticity law (*c.f.*, Figure 2). The nonlinear models deform much less than the linear model overall.

We examine the rate of deformation in Figure 5. All three models relax exponentially toward their respective steady states, but the rate of relaxation depends very strongly on the magnitude of the applied effective stress and on the nonlinearities of the model. Specifically, the nonlinear- k_0 model relaxes much faster than the linear model, whereas the nonlinear- k_{KC} model relaxes much more slowly than the linear model. The relaxation timescale τ , which is the characteristic time associated with the decaying exponentials shown in Figure 5, is constant for the linear model, but decreases with $|\sigma^*|$ for the nonlinear- k_0 model and increases strongly with $|\sigma^*|$ for the nonlinear- k_{KC} model (Figure 6). The timescales of the nonlinear models differ from that of the linear model by several-fold for moderate strain.

VI. FLUID-DRIVEN DEFORMATION

We now consider the uniaxial deformation of a porous material driven by a net fluid flow through the material from left to right (Figure 1c), which compresses the material against the rigid right boundary. This problem has attracted interest since the 1970s for applications in filtration and the manufacturing of composites [*e.g.*, 70, 73, 76, 77, 80], in tissue mechanics [*e.g.*, 68, 69], and as a convenient model problem in poroelasticity [*e.g.*, 78, 84–86].

We assume that a pressure drop Δp^* is suddenly ap-

plied across the material at $t = 0^+$, and we write this as $p(\delta, t) = \Delta p^*$ and $p(L, t) = 0$ without loss of generality. We also assume for simplicity that the left edge is unconstrained, $\sigma'(\delta, t) = 0$, but our models and solutions do not require this. Force balance then leads to $\sigma'(L, t) = -\Delta p^*$, implying that the right edge of the skeleton is compressed against the right boundary.

As in the consolidation problem, the deformation will evolve toward a state in which the solid is stationary. Unlike in the consolidation problem, fluid flow is central to this steady state because the flow drives the deformation. The resulting deformation field is highly nonuniform because it must balance the internal pressure gradient. As discussed in §IV B 3 above, the same steady state can be achieved when the flow is instead driven by an imposed fluid flux q^* ; we focus on the case of an applied pressure drop here for simplicity, but our models and solutions are general and can also be used for the case of an imposed flux.

A. Steady state

The deformation will eventually reach a state in which the flow is steady ($q(t) \rightarrow q^*$ and $v_f(x, t) \rightarrow v_f(x)$) and the solid is stationary ($v_s \rightarrow 0$ and $\phi_f v_f \rightarrow q^*$). We present in Appendix D a general procedure for constructing steady-state solutions to the kinematically exact model for arbitrary elasticity and permeability laws, and we provide the key results for the two nonlinear models and the two intermediate models in Appendix F. Below, we discuss the results for the nonlinear- k_0 model and the linear model.

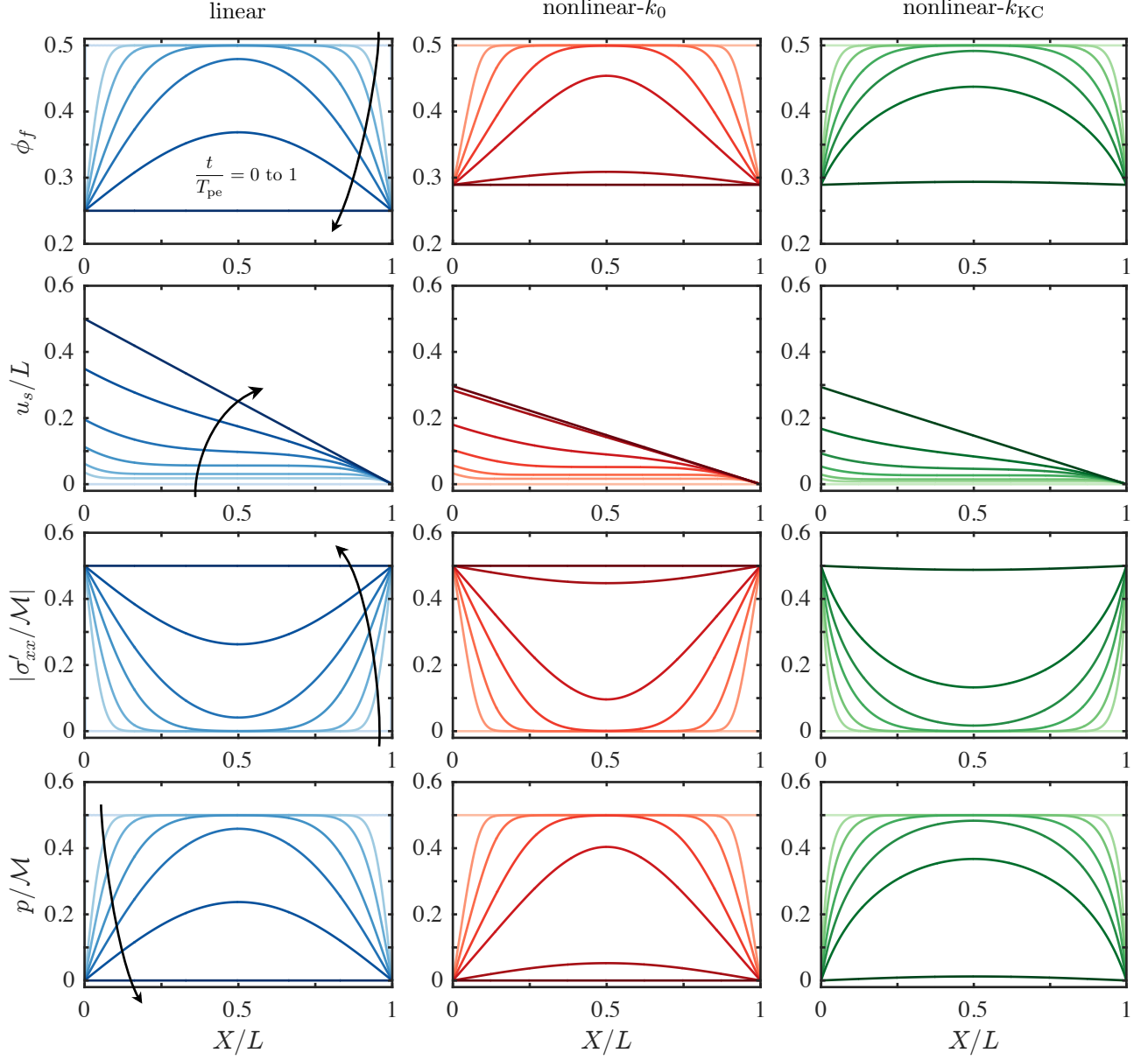


FIG. 4. Dynamics of the consolidation process for a soft porous material under an applied effective stress of $\sigma'^*/\mathcal{M} = -0.5$. We show the porosity (first row), displacement (second row), effective stress (third row), and pressure (last row) at $t/T_{pe} = 0, 0.001, 0.003, 0.01, 0.03, 0.1, \text{ and } 1$, as indicated (light to dark colors), for the linear model (left column, blue), the nonlinear- k_0 model (middle column, red), and the nonlinear- k_{KC} model (right column, green). For the nonlinear models, we plot these results against the Lagrangian coordinate $X = x - u_s(x, t)$ for clarity; for the linear model, we again adopt a Lagrangian interpretation and simply replace x with X in the relevant expressions (see §III C and §V B). These results are for $\phi_{f,0} = 0.5$.

For the nonlinear- k_0 model, the pressure and effective stress fields can be calculated by integrating Equa-

tion (31b) or (31c) with (31d),

$$\frac{p(x)}{\mathcal{M}} = \frac{\mu q^* L}{k_0 \mathcal{M}} \left(1 - \frac{x}{L}\right), \quad (56a)$$

$$\frac{\sigma'_{xx}(x)}{\mathcal{M}} = -\frac{\mu q^* L}{k_0 \mathcal{M}} \left(\frac{x}{L} - \frac{\delta^*}{L}\right). \quad (56b)$$

Since the permeability is constant, the pressure drops

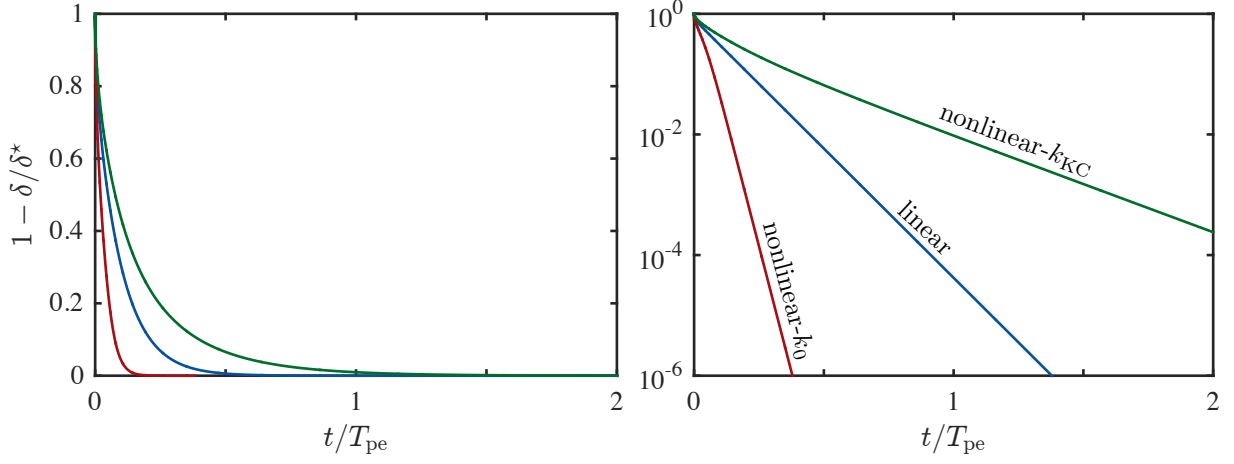


FIG. 5. Relaxation of the deflection δ toward its steady-state value δ^* during consolidation for $\sigma'^*/\mathcal{M} = -0.5$ on a linear scale (left) and on a semilogarithmic scale (right). We again show the linear model (blue), the nonlinear- k_0 model (red), and the nonlinear- k_{KC} model (green). All three models relax exponentially, but the nonlinear- k_0 model relaxes about 4 times faster than the linear model, whereas the nonlinear- k_{KC} model relaxes at less than half the rate of the linear model. These results are for $\phi_{f,0} = 0.5$.

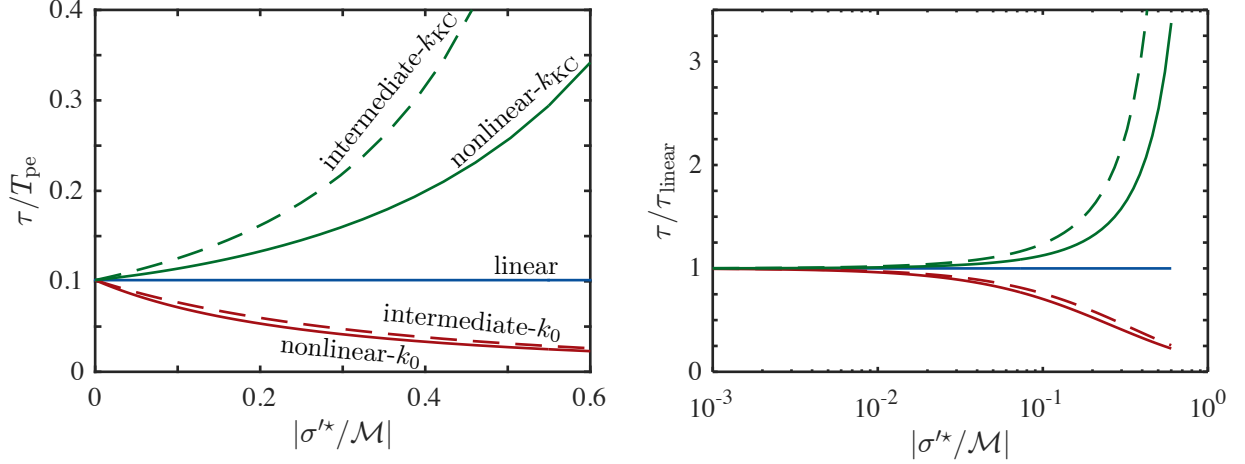


FIG. 6. The consolidation timescale is constant and equal to π^{-2} for the linear model, but depends strongly on the magnitude of the applied effective stress for the nonlinear models. Here, we plot (left) the timescale τ/T_{pe} against the magnitude of the applied effective stress $|\sigma'^*/\mathcal{M}|$ on a linear scale for the linear model (solid blue), the nonlinear- k_0 model (solid red), the nonlinear- k_{KC} model (solid green), the intermediate- k_0 model (dashed red), and the intermediate- k_{KC} model (dashed green). We also compare the relaxation timescales of all models with that of the linear model by plotting (right) τ/τ_{linear} against $|\sigma'^*/\mathcal{M}|$ on a semilogarithmic scale. The nonlinear and intermediate models with constant permeability always relax much faster than the linear model, whereas those with deformation-dependent permeability always relax much more slowly than the linear model. These results are for $\phi_{f,0} = 0.5$.

linearly from $p(\delta^*) = \Delta p^*$ to $p(L) = 0$. The effective stress must therefore also vary linearly in x , rising in magnitude from $\sigma'_{xx}(\delta^*) = 0$ to $\sigma'_{xx}(L) = -\Delta p^*$. The total stress is uniform and equal to $\sigma_{xx}(x) = \sigma'_{xx}(x) - p(x) = -\Delta p^*$, and this is supported entirely by the fluid at the left and entirely by the skeleton at the right.

The unknown flux q^* can be calculated directly from

(see Appendix D)

$$\frac{\mu q^* L}{k_0 \mathcal{M}} = \frac{1}{4} \left(\frac{1}{J(L)^2} - 1 \right) - \left(\frac{1}{2J(L)} \right) \frac{\ln J(L)}{J(L)}, \quad (57)$$

where $J(L) = (1 - \phi_{f,0})/(1 - \phi_f(L))$ is the Jacobian determinant at $x = L$, which is readily calculated by inverting $\sigma'_{xx}(\phi_f(L)) = -\Delta p^*$ using the elasticity law (Equation 38). For an imposed flux, Equation (57) should instead be solved for $J(L)$, which will then provide Δp^* .

The unknown deflection δ^* can then be calculated by evaluating the pressure at $x = \delta^*$ or the effective stress at $x = L$, both of which lead to

$$\frac{\delta^*}{L} = 1 - \left(\frac{\Delta p^*}{\mathcal{M}} \right) \left(\frac{k_0 \mathcal{M}}{\mu q^* L} \right). \quad (58)$$

We can then calculate the Jacobian determinant field $J(x)$ from the effective stress field using Equation (38),

$$J(x) = - \left[\frac{\mu q^* L}{k_0 \mathcal{M}} \left(\frac{x}{L} - \frac{\delta^*}{L} \right) \right]^{-1} \text{W} \left[- \frac{\mu q^* L}{k_0 \mathcal{M}} \left(\frac{x}{L} - \frac{\delta^*}{L} \right) \right], \quad (59)$$

where $\text{W}(\cdot)$ is again the Lambert W function. The porosity field $\phi_f(x)$ is again given by,

$$\phi_f(x) = 1 - \frac{1 - \phi_{f,0}}{J(x)} \quad (60)$$

and, finally, the displacement field is

$$\frac{u_s(x)}{L} = \frac{\delta^*}{L} - \frac{k_0 \mathcal{M}}{\mu q^* L} \left[\frac{1}{4} \left(\frac{1}{J(x)^2} - 1 \right) - \frac{1}{2} \left(\frac{1}{J(x)} - 2 \right) \frac{\ln J(x)}{J(x)} \right]. \quad (61)$$

The linear model is, of course, much simpler. The pressure and effective stress fields are similar to those for the nonlinear- k_0 model,

$$\frac{p(x)}{\mathcal{M}} \approx \frac{\mu q^* L}{k_0 \mathcal{M}} \left(1 - \frac{x}{L} \right), \quad (62a)$$

$$\frac{\sigma'_{xx}(x)}{\mathcal{M}} \approx - \frac{\mu q^* L}{k_0 \mathcal{M}} \left(\frac{x}{L} \right). \quad (62b)$$

Evaluating the pressure at $x \approx 0$ or the effective stress at $x = L$ immediately provides the relationship between the flux and the pressure drop,

$$\frac{\mu q^* L}{k_0 \mathcal{M}} \approx \frac{\Delta p^*}{\mathcal{M}}. \quad (63)$$

The porosity field is calculated from the effective stress field and linear elasticity,

$$\frac{\phi_f(x) - \phi_{f,0}}{1 - \phi_{f,0}} \approx - \frac{\mu q^* L}{k_0 \mathcal{M}} \left(\frac{x}{L} \right), \quad (64)$$

and the displacement field is calculated by integrating the porosity field,

$$\frac{u_s(x)}{L} \approx \frac{\mu q^* L}{2k_0 \mathcal{M}} \left(1 - \frac{x}{L} \right)^2. \quad (65)$$

Since the stress and therefore the strain increase linearly from left to right, the displacement is quadratic. Finally, the deflection is simply given by $\delta^* \approx u_s(0)$,

$$\frac{\delta^*}{L} \approx \frac{1}{2} \frac{\mu q^* L}{k_0 \mathcal{M}}. \quad (66)$$

We compare these predictions qualitatively in Figure 7, including also the results for the nonlinear- k_{KC} model. As with consolidation, the nonlinear models deform less than the linear model in all cases. Unlike with consolidation, the permeability law has a strong impact on the steady state: The nonlinear- k_{KC} model deforms less than the nonlinear- k_0 model, and exhibits more strongly nonlinear behavior. We compare the predictions for the final deflection δ^* and the resulting flux q^* in Figure 8, including also the two intermediate models. Although all of the nonlinear and intermediate models predict a much smaller deflection than the linear model, the nonlinear- k_0 and intermediate- k_0 models predict a larger steady-state flux than the linear model, whereas the nonlinear- k_{KC} and intermediate- k_{KC} models predict a much smaller steady-state flux. This occurs because the steady-state flux results from two competing physical effects. As the driving pressure drop increases, we expect the deflection to increase. As the deflection increases, the overall length of the skeleton decreases and, since the pressure drop is fixed, the pressure gradient across the material increases. As a result, we expect from Darcy's law that the flux will scale like $q^* \sim (k/\mu)\Delta p^*/(L - \delta^*)$. For constant permeability, we therefore expect the flux to increase faster-than-linearly with Δp^* , and this is indeed what we see for the nonlinear- k_0 and intermediate- k_0 cases. The changing length is a kinematic nonlinearity that is neglected in the linear model, so q_{linear}^* is simply proportional to Δp^* despite the fact that δ_{linear}^* is actually larger than the nonlinear or intermediate predictions. However, these models ignore the fact that the porosity decreases as the deformation increases. When the permeability is deformation-dependent, this decreases very strongly with the porosity and overwhelms the effect of the changing length, leading to a strongly slower-than-linear growth of q^* with Δp^* , and this is indeed what we see for the nonlinear- k_{KC} and intermediate- k_{KC} models.

1. Dynamics

We next focus on the dynamic evolution of the deformation. We again solve the nonlinear and intermediate models numerically (Appendix C and [79]), and we again solve the linear model analytically via separation of variables. The analytical solution can be written

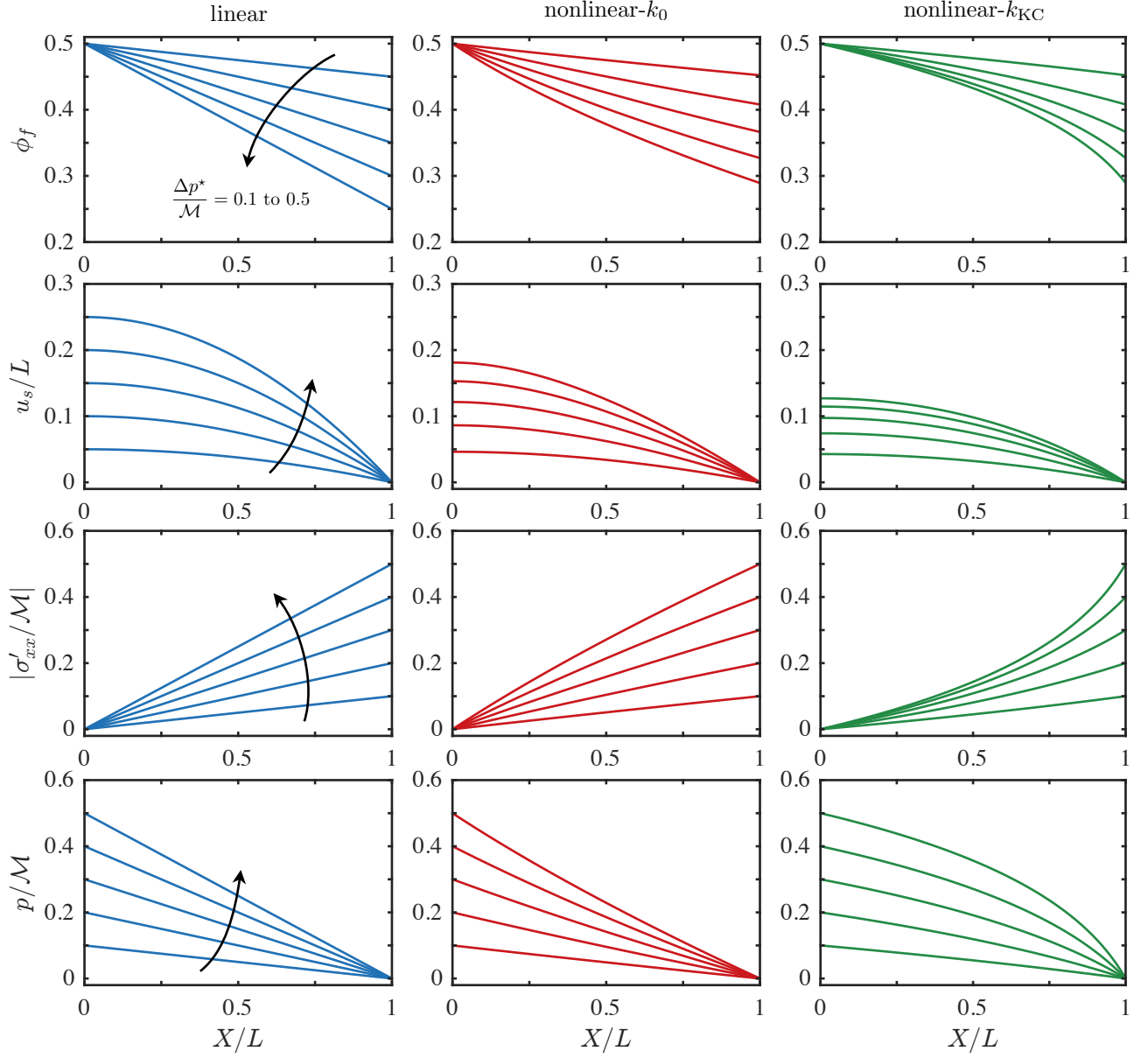


FIG. 7. Steady-state in fluid-driven deformation of a soft porous material, where fluid flow through the material from left to right is driven by an imposed pressure drop Δp^* . Here, we show the results for $\Delta p^*/\mathcal{M}$ increasing from 0.1 to 0.5, as indicated. We show the porosity (first row), displacement (second row), effective stress (third row), and pressure (last row) for the linear model (left column, blue), the nonlinear- k_0 model (middle column, red), and the nonlinear- k_{KC} model (right column, green). For the nonlinear models, we again plot these results against the Lagrangian coordinate $X = x - u_s(x, t)$ for clarity; for the linear model, we again adopt a Lagrangian interpretation of the spatial coordinate. The nonlinear models deform less than the linear model in all cases, with the nonlinear- k_{KC} model deforming the least but exhibiting the most strongly nonlinear behavior. These results are for $\phi_{f,0} = 0.5$.

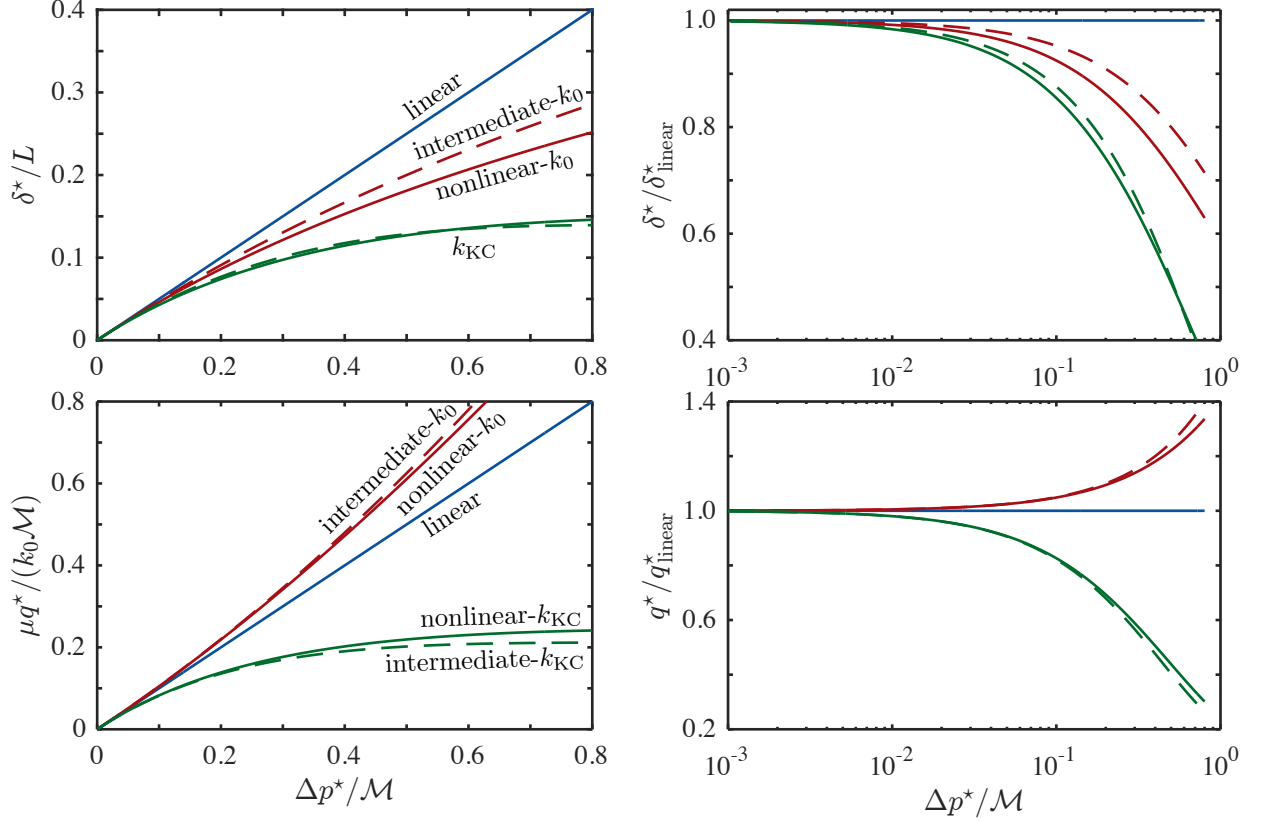


FIG. 8. The linear model over-predicts the steady-state deformation relative to the nonlinear models during fluid-driven deformation. For flow driven by an applied pressure drop Δp^* , we plot here the steady-state deflection δ^* (top row) and the steady-state fluid flux q^* (bottom row) against Δp^* on a linear scale (left column) for the linear model (solid blue), the nonlinear- k_0 model (solid red), the nonlinear- k_{KC} model (solid green), the intermediate- k_0 model (dashed red), and the intermediate- k_{KC} model (dashed green). We also compare (right) the deflection and flux for all models with that of the linear model, $\delta^*/\delta^*_{\text{linear}}$ and q^*/q^*_{linear} , on a semilogarithmic scale. The nonlinear- k_0 and intermediate- k_0 models predict a somewhat higher flux than the linear model due to kinematic nonlinearity, but the nonlinear- k_{KC} and intermediate- k_{KC} models predict a much lower flux than the linear model because the permeability decreases strongly as the pressure drop increases, leading to a much lower flux for a given pressure drop.

$$\phi_f(x, t) = \phi_{f,0} + (\phi_f^* - \phi_{f,0}) \left\{ \frac{x}{L} + \sum_{n=1}^{\infty} \frac{2}{n\pi} [(-1)^n] e^{-\frac{(n\pi)^2 t}{T_{pe}}} \sin\left(\frac{n\pi x}{L}\right) \right\}, \quad (67a)$$

$$\frac{u_s(x, t)}{L} = - \left(\frac{\phi_f^* - \phi_{f,0}}{1 - \phi_{f,0}} \right) \left\{ \frac{1}{2} \left[1 - \left(\frac{x}{L} \right)^2 \right] - \sum_{n=1}^{\infty} \frac{2}{(n\pi)^2} [(-1)^n] e^{-\frac{(n\pi)^2 t}{T_{pe}}} \left[(-1)^n - \cos\left(\frac{n\pi x}{L}\right) \right] \right\}, \quad (67b)$$

where $\phi_f(0, t) = \phi_{f,0}$ and $\phi_f(L, t) = \phi_f^* = \phi_{f,0} - (1 - \phi_{f,0})(\Delta p^*/\mathcal{M})$. We compare these solutions qualitatively in Figure 9, including also the results for the nonlinear- k_{KC} case. Note once again that the spatial coordinate in the linear model is ambiguous, and we again adopt a Lagrangian interpretation.

When the flow starts, the fluid and the solid initially travel together to the right. The pressure remains uni-

form throughout most of the skeleton since there is no net flux of fluid *through* the skeleton, but there is a very sharp pressure gradient at the right edge where the solid is necessarily stationary. The motion of the solid toward the right boundary gradually compresses the right edge of the skeleton against the boundary, and this motion slows over time as the effective stress builds from right to left. The motion of the solid eventually stops and the

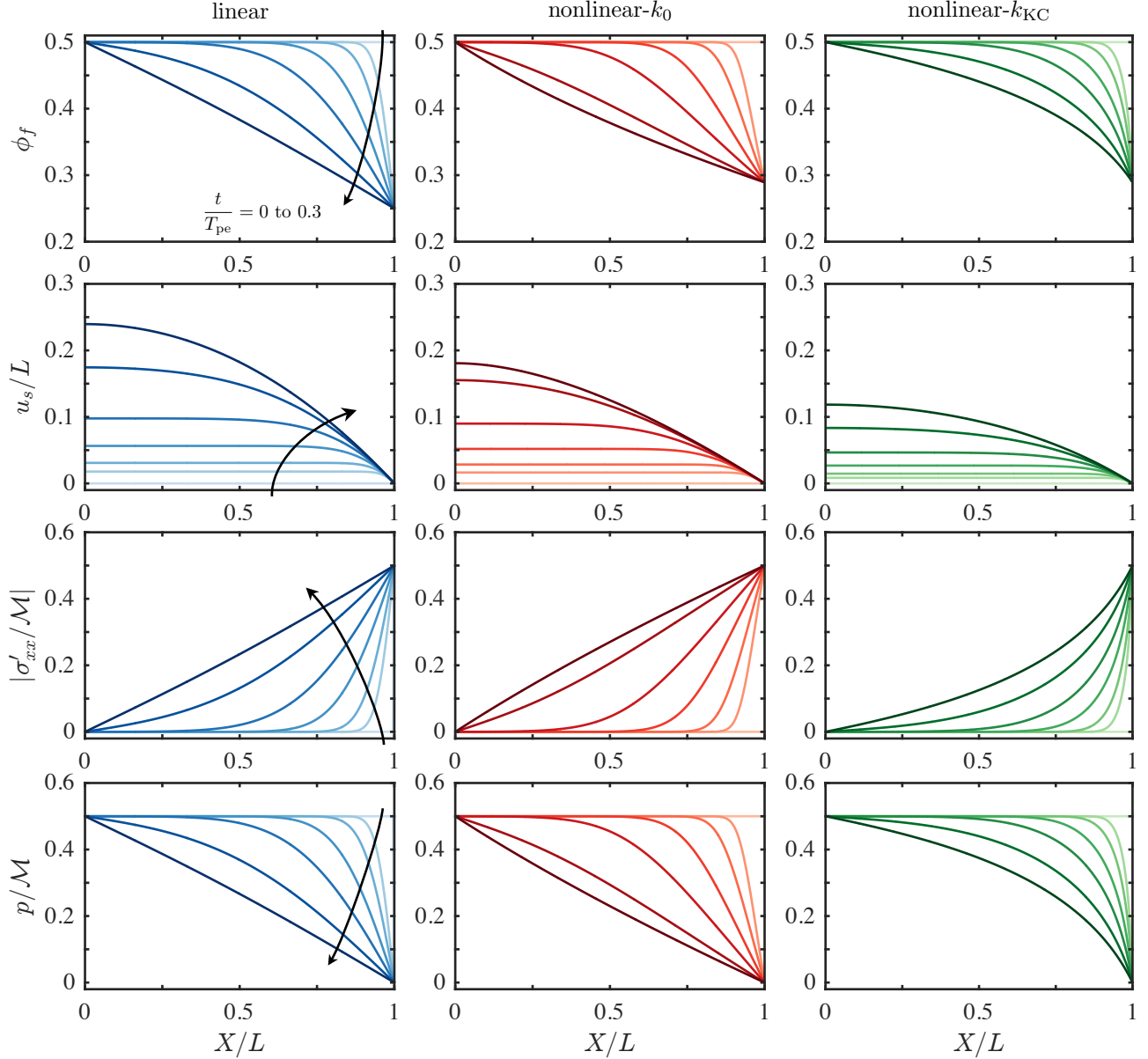


FIG. 9. Dynamics of fluid-driven deformation for a soft porous material, where the net flow from left to right is driven by an applied pressure drop $\Delta p^* = 0.5$. We show the porosity (first row), displacement (second row), effective stress (third row), and pressure (last row) at $t/T_{pe} = 0, 0.001, 0.003, 0.01, 0.03, 0.1,$ and 0.3 , as indicated (light to dark colors), for the linear model (left column, blue), the nonlinear- k_0 model (middle column, red), and the nonlinear- k_{KC} model (right column, green). For the nonlinear models, we plot these results against the Lagrangian coordinate $X = x - u_s(x, t)$ for clarity; for the linear model, we again adopt a Lagrangian interpretation and simply replace x with X in the relevant expressions (see §III C and §V B). These results are for $\phi_{f,0} = 0.5$.

deformation reaches steady state when the strain in the skeleton is such that the gradient in effective stress balances the gradient in pressure. In this steady state, the skeleton remains completely relaxed at the left edge and is the most compressed at the right edge, transition from left to right with a gradual increase in deformation and

magnitude of effective stress, and a gradual decrease in pressure and porosity.

Both here and in the consolidation problem, the deformation evolves with a classic boundary-layer structure that may be susceptible to a matched asymptotic approach with t/T_{pe} the small parameter. The prospect

of more accurately capturing the kinematic nonlinearity while retaining some degree of analytical tractability is a promising one for future work.

To examine the timescale of the deformation, we plot the evolution of the deflection toward its final value as a proxy for the global approach to steady state (Figure 10). As for consolidation, we find that the deflection approaches steady state exponentially in all cases, and that the nonlinear- k_0 and nonlinear- k_{KC} models evolve more quickly and more slowly than the linear model, respectively. We also investigate the impact of Δp^* on the timescale (Figure 11). We find that the general trend is the same as in consolidation (*c.f.*, Figure 6), but that the magnitude of the effect is smaller—That is, the timescale during fluid-driven deformation depends less strongly on Δp^* than the timescale during consolidation depends on σ^* . This is most likely due to the fact that the steady-state is uniform in consolidation, with potentially large compression throughout the entire material, whereas the steady-state in fluid-driven deformation is highly nonuniform, with completely relaxed material at the left and highly compressed material at the right.

VII. DISCUSSION & CONCLUSIONS

We have provided an overview and discussion of a complete Eulerian framework for the arbitrarily large deformation of a porous material. In doing so, our main goals were to (a) elucidate the key aspects of the rigorous model, (b) provide physical insight into the subtleties of poromechanical coupling, and (c) investigate the qualitative and quantitative nature of the error introduced by linearizing this model. These points are often obscured by the powerful mathematical and computational machinery that is typically brought to bear on these problems. We intend that our approach here can serve as a concise, coherent, and approachable introduction to a large body of work in classical continuum and poromechanics. We believe that this now provides a rostrum to facilitate further theoretical advances and new applications in soil mechanics, hydrogeology, biophysics, and biomedical engineering.

We have also applied this theory to two canonical model problems in uniaxial deformation, one in which deformation drives fluid flow and one in which fluid flow drives deformation. In the former, the consolidation problem, an applied effective stress squeezes fluid from a porous material. Although the steady-state is simple and controlled entirely by the solid mechanics, the evolution of the deformation is controlled by the rate at which fluid can flow through the material and out at the boundaries; we showed that the resulting rate of relaxation is impacted strongly by kinematic nonlinearity and even more strongly by deformation-dependent permeability. In the latter problem, fluid-driven deformation, a net through-flow compresses the material against a rigid permeable boundary. The steady-state is highly

nonuniform, controlled by the steady balance between the gradient in pressure and the gradient in stress. We showed that both the evolution of the deformation and the deflection and fluid flux at steady-state are impacted strongly by kinematic nonlinearity and, again, even more strongly by deformation-dependent permeability.

In the interest of emphasizing the nonlinear kinematics of large deformations, we have avoided complex, material-specific constitutive models. Hencky elasticity captures the full kinematic nonlinearity of large deformations in a very simple form, and we believe that it provides a reasonable compromise between rigor and complexity for moderate deformations. However, real materials will always behave in a complex, material-specific way when subject to sufficiently large strains, and the framework considered here is fully compatible with other constitutive models. Similarly, we have considered one specific case of deformation-dependent permeability: The normalized Kozeny-Carman formula. We have shown that this typically amplifies the importance of kinematic nonlinearity and has striking qualitative and quantitative impacts on poromechanical behavior. Although this example captures the key qualitative features of the coupling between deformation and permeability, material-specific relationships will be needed to provide quantitative predictions for real materials.

In describing the kinematics of the solid skeleton, we have adopted the single assumption that the constituent material is incompressible. This has clear relevance to soil mechanics and biophysics, but also in any situation where the pressure and stress are small compared to the bulk modulus of the solid grains (*e.g.*, $\sim 30\text{--}40$ GPa for quartz sand). This assumption can be relaxed, although doing so substantially complicates the large-deformation theory [*e.g.*, 32, 50, 52]. We have also focused on the case of a single, incompressible pore fluid, but the theory is readily generalized to a compressible or multiphase fluid system [*e.g.*, 32, 43].

Uniaxial deformations have provided a convenient testbed for our purposes here, but they are unusual in several respects that do not readily generalize to multi-axial scenarios. Firstly, a uniaxial deformation can be fully characterized by the change in porosity, $\sigma'_{xx} = \sigma'_{xx}(\phi_f)$; this simplifies the analysis, but it is not the case for even simple biaxial deformations. Secondly, the cross-section normal to the flow does not deform or rotate, which greatly simplifies the nonlinearity of poromechanical coupling. Finally, the exact relationship between displacement and porosity is linear; this is again not the case for even simple biaxial deformations. We expect kinematic nonlinearity to play an even stronger role for multi-axial deformations.

The authors gratefully acknowledge support from the Yale Climate & Energy Institute. ERD acknowledges support from the National Science Foundation (Grant No. CBET-1236086). JSW acknowledges support from Yale University, the Swedish Research Council (Vetenskapsrådet grant 638-2013-9243), and a Royal Society

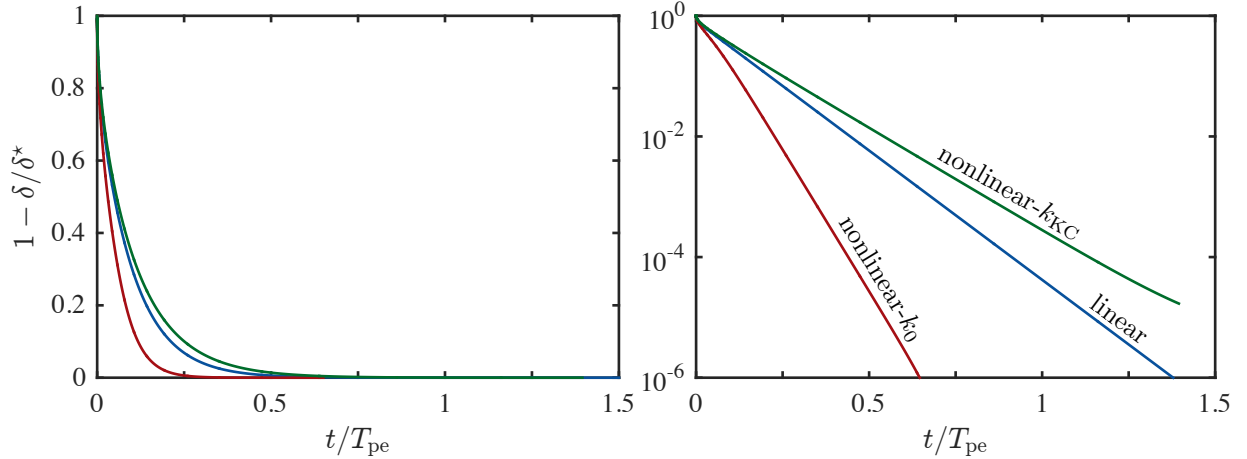


FIG. 10. Relaxation toward steady-state during fluid-driven deformation with $\Delta p^*/\mathcal{M} = 0.5$ on a linear scale (left) and on a semilogarithmic scale (right). We plot the relative difference between $\delta(t)$ and its final value δ^* as a proxy for the global approach to steady state. We show again the linear (blue), nonlinear- k_0 (red), and nonlinear- k_{KC} (green) models. The final deflection δ^* is largest for the linear model, followed by the nonlinear- k_0 model, followed by the nonlinear- k_{KC} model ($\delta^* = 0.25$, 0.181, and 0.127, respectively; *c.f.*, Figure 8). As with consolidation, however, the nonlinear- k_0 model relaxes more quickly than linear model (at more than twice the rate), whereas the nonlinear- k_{KC} model relaxes more slowly than the linear model (at about 80% of the rate; *c.f.*, Figure 5). These results are for $\phi_{f,0} = 0.5$.

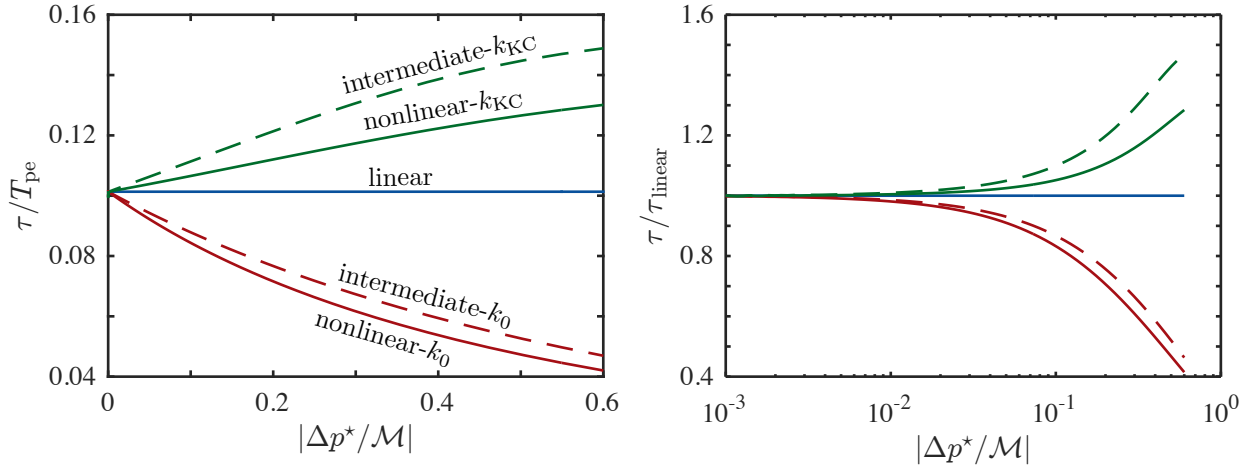


FIG. 11. The deformation approaches steady state more quickly for larger Δp^* when the permeability is constant, and more slowly for larger Δp^* when the permeability is deformation-dependent. Here, we plot (left) the relaxation timescale τ/T_{pe} against Δp^* for the linear (solid blue), nonlinear- k_0 (solid red), nonlinear- k_{KC} (solid green), intermediate- k_0 (dashed red), and intermediate- k_{KC} (dashed green) models. The timescale is constant and equal to π^{-2} for the linear model, but increases with Δp^* for the two k_0 models and decreases with Δp^* for the two k_{KC} models. We also compare the relaxation timescales of all models with that of the linear model by plotting (right) τ/τ_{linear} on a semilogarithmic scale. These results are for $\phi_{f,0} = 0.5$.

Wolfson Research Merit Award.

Appendix A: Large-deformation poroelasticity in a Lagrangian framework

Here we briefly summarize the Lagrangian approach to large-deformation poroelasticity, a thorough discussion and derivation of which is provided by Coussy [32]. In a Lagrangian frame, it is natural to work with so-

called *nominal* quantities, which measure the current stresses, fluxes, *etc.* acting on or through the reference (initial/relaxed) areas or volumes. For example, the nominal porosity Φ_f measures the current fluid volume per unit reference total volume, and is related to the true porosity via $\Phi_f = J\phi_f$. We denote the gradient and divergence operators in the Lagrangian coordinate system by $\text{grad}(\cdot)$ and $\text{div}(\cdot)$, respectively, to distinguish them from the corresponding operators in the Eulerian coordi-

nate system. The Lagrangian displacement field is

$$\mathbf{U}_s = \mathbf{x}(\mathbf{X}, t) - \mathbf{X}, \quad (\text{A1})$$

where \mathbf{X} is the Lagrangian (material) coordinate and $\mathbf{x}(\mathbf{X}, t)$ is the current position of the skeleton that was initially at position \mathbf{X} . The corresponding deformation-gradient tensor is

$$\mathbf{F} = \text{grad}(\mathbf{x}) = \mathbf{I} + \text{grad}(\mathbf{U}_s). \quad (\text{A2})$$

The Jacobian determinant is then related to Φ_f by

$$J = \det(\mathbf{F}) = 1 + \Phi_f - \Phi_{f,0}, \quad (\text{A3})$$

where $\Phi_{f,0}(\mathbf{X})$ is the reference porosity field, which we again take to be undeformed. Continuity requires that

$$\frac{\partial \Phi_f}{\partial t} + \text{div}(\mathbf{W}_f) = 0, \quad (\text{A4})$$

where \mathbf{W}_f is the nominal flux of fluid through the solid skeleton. The nominal flux is related to the pressure gradient via Darcy's law,

$$\mathbf{W}_f = -J\mathbf{F}^{-1}\mathbf{F}^{-\top} \cdot \frac{k(\phi_f)}{\mu} \text{grad}(p), \quad (\text{A5})$$

where the $J\mathbf{F}^{-1}$ portion of the prefactor converts the true flux to the nominal flux, and the remaining factor of $\mathbf{F}^{-\top}$ converts the Eulerian gradient to the Lagrangian one. Mechanical equilibrium requires that

$$\text{div}(\mathbf{s}) = 0, \quad (\text{A6})$$

where \mathbf{s} is the nominal total stress. This is related to the true total stress via

$$\mathbf{s} = J\boldsymbol{\sigma}\mathbf{F}^{-\top}. \quad (\text{A7})$$

The nominal effective stress \mathbf{s}' is then given by

$$\mathbf{s}' = \mathbf{s} + J\mathbf{F}^{-\top}p. \quad (\text{A8})$$

Combining Equations (A4)–(A8), we finally have

$$\frac{\partial \Phi_f}{\partial t} - \text{div} \left[J\mathbf{F}^{-1}\mathbf{F}^{-\top} \cdot \frac{k(\phi_f)}{\mu} \text{grad}(p) \right] = 0 \quad \text{and} \quad (\text{A9a})$$

$$\text{div}(\mathbf{s}') = \text{div}(J\mathbf{F}^{-\top}p). \quad (\text{A9b})$$

Supplemented with a constitutive law for the solid skeleton (relating \mathbf{s}' to \mathbf{U}_s) and appropriate boundary conditions, this constitutes a complete formulation of poroelasticity in a Lagrangian framework [32]. This is more suitable for computation than the Eulerian interpretation since the domain is fixed, but the underlying physical structure is substantially more opaque. Note that the permeability must remain a function of the true porosity, $k = k(\phi_f) = k(\Phi_f/J)$.

Linearizing Equations (A9) in the strain leads to

$$\frac{\partial \phi_f}{\partial t} - \text{div} \left[(1 - \phi_{f,0}) \frac{k_0}{\mu} \text{grad}(p) \right] \approx 0 \quad \text{and} \quad (\text{A10a})$$

$$\text{div}(\sigma') \approx \text{grad}(p), \quad (\text{A10b})$$

which coincide with Equations (24) and (19), respectively, but replacing \mathbf{x} with \mathbf{X} . Note that we have reverted from the nominal porosity to the true porosity, and that these two differ *at leading order*:

$$\Phi_f - \Phi_{f,0} = \frac{\phi_f - \phi_{f,0}}{1 - \phi_f} \approx \frac{\phi_f - \phi_{f,0}}{1 - \phi_{f,0}}, \quad (\text{A11})$$

where the reference fields are always precisely equivalent, $\Phi_{f,0} \equiv \phi_{f,0}$, because they must necessarily refer to the same reference state.

Appendix B: Eulerian and Lagrangian interpretations of linear elasticity

The Eulerian (Eulerian-Almansi) and Lagrangian (Green-Lagrange) finite-strain tensors are

$$\mathbf{e} = \frac{1}{2}(\mathbf{I} - \mathbf{B}^{-1}) = \frac{1}{2}(\mathbf{I} - \mathbf{F}^{-\top}\mathbf{F}^{-1}) \quad (\text{B1})$$

and

$$\mathbf{E} = \frac{1}{2}(\mathbf{C} - \mathbf{I}) = \frac{1}{2}(\mathbf{F}^\top\mathbf{F} - \mathbf{I}), \quad (\text{B2})$$

respectively. Linear elasticity, as described above, is effectively a linearized Eulerian constitutive law, where stress is linear in Eulerian strain $\partial u/\partial x$. This can be written as

$$\boldsymbol{\varepsilon}_e = \frac{1}{2} \left[\frac{\partial \mathbf{u}_s}{\partial \mathbf{x}} + \left(\frac{\partial \mathbf{u}_s}{\partial \mathbf{x}} \right)^\top \right] = \mathbf{I} - \frac{1}{2}(\mathbf{F}^{-1} + \mathbf{F}^{-\top}). \quad (\text{B3})$$

However, a linearized Lagrangian constitutive law, where stress is linear in Lagrangian strain $\partial u/\partial X$, is equally valid, and can be written as

$$\boldsymbol{\varepsilon}_E = \frac{1}{2} \left[\frac{\partial \mathbf{u}_s}{\partial \mathbf{X}} + \left(\frac{\partial \mathbf{u}_s}{\partial \mathbf{X}} \right)^\top \right] = \frac{1}{2}(\mathbf{F} + \mathbf{F}^\top) - \mathbf{I}. \quad (\text{B4})$$

The former is nonlinear in a Lagrangian frame whereas the latter is nonlinear in an Eulerian frame. We used the linearized Eulerian law above, but in a Lagrangian frame it would be more appropriate to use the linearized Lagrangian law. The results are equivalent at leading order in the strain ($\partial u/\partial x \approx \partial u/\partial X$), but they diverge as strains become non-negligible.

Appendix C: Finite-volume method with a moving boundary

To solve Equation (31a) numerically, we formulate a finite-volume method on an adaptive grid. We provide a reference implementation in the Supplemental Material [79]. At any time t , the domain extends from

$x = \delta(t)$ to $x = L$. We divide this into N cells of equal width $\Delta x(t) = [L - \delta(t)]/N$, where cell i has center $x_i(t) = \delta(t) + (i - 1/2)\Delta x(t)$ and we denote its left and right edges by $x_{i-1/2}(t) = x_i(t) - \Delta x(t)/2$ and $x_{i+1/2}(t) = x_i(t) + \Delta x(t)/2$, respectively. Making use of the expressions

$$\frac{\partial}{\partial t} \Delta x = -\frac{1}{N} \frac{d\delta}{dt} = -\frac{\Delta x}{L - \delta} \dot{\delta} \quad \text{and} \quad (\text{C1a})$$

$$\frac{\partial}{\partial t} x_i = \frac{L - x_i}{L - \delta} \dot{\delta}, \quad (\text{C1b})$$

we formulate a finite-volume method in the standard way [e.g., 87], integrating Equation (31a) over cell i ,

$$\int_{x_{i-1/2}}^{x_{i+1/2}} \left\{ \frac{\partial \phi_f}{\partial t} + \frac{\partial}{\partial x} [\phi_f v_f] \right\} dx = 0, \quad (\text{C2})$$

where

$$\phi_f v_f = \phi_f q(t) - (1 - \phi_f) \frac{k(\phi_f)}{\mu} \frac{\partial p}{\partial x}, \quad (\text{C3})$$

as derived above. We arrive at

$$\int_{x_{i-1/2}}^{x_{i+1/2}} \frac{\partial \phi_f}{\partial t} dx + \left[\phi_f v_f \right]_{x_{i-1/2}}^{x_{i+1/2}} = 0. \quad (\text{C4})$$

After manipulating the first term using the Leibniz integral rule and regrouping, we have

$$\frac{\partial}{\partial t} \int_{x_{i-1/2}}^{x_{i+1/2}} \phi_f dx + \left[-\left(\frac{L-x}{L-\delta} \right) \phi_f \dot{\delta} + \phi_f v_f \right]_{x_{i-1/2}}^{x_{i+1/2}} = 0. \quad (\text{C5})$$

Defining $\phi_{f,i}$ to be the average of ϕ_f within cell i ,

$$\phi_{f,i} \equiv \frac{1}{\Delta x} \int_{x_{i-1/2}}^{x_{i+1/2}} \phi_f dx, \quad (\text{C6})$$

we finally have

$$\begin{aligned} \frac{\partial \phi_{f,i}}{\partial t} - \left(\frac{\dot{\delta}}{L - \delta} \right) \phi_{f,i} \\ + \frac{1}{\Delta x} \left[-\left(\frac{L-x}{L-\delta} \right) \phi_f \dot{\delta} + \phi_f v_f \right]_{x_{i-1/2}}^{x_{i+1/2}} = 0. \end{aligned} \quad (\text{C7})$$

We discretize the quantity in square brackets by upwinding the advective components and using a centered difference for the diffusive components. Simultaneously, we must also solve an evolution equation for the position of the moving boundary. This comes from Equation (31c) and (35),

$$\dot{\delta} = q(t) + \left(\frac{k(\phi_f)}{\mu} \frac{\partial p}{\partial x} \right) \Big|_{x=\delta}. \quad (\text{C8})$$

This system can be written directly in terms of the porosity once a stress-strain constitutive law is specified, at which point we have a closed set of equations in ϕ_f and δ . We integrate these equations in time using an explicit Runge-Kutta scheme.

Appendix D: Steady-state solutions: General procedure

In steady state, it is possible to construct (usually implicit) analytical solutions for any combination of elasticity and permeability law. We outline the general procedure below and provide a reference implementation in the Supplemental Material [79]. Barry and Aldis [88] suggested a somewhat similar procedure for axisymmetric geometries [c.f., §5 of Ref. 88].

Of the four quantities σ'^* , q^* , Δp^* , and δ^* , two must be known in advance. We assume here that these are σ'^* and either q^* or Δp^* , but it is straightforward to adapt or invert this procedure for other pairs. This procedure degenerates when there is no flow at steady state, $q^* = 0 \leftrightarrow \Delta p^* = 0$, as in consolidation. The solution in this case depends only on the solid mechanics, and is very straightforward to derive directly from the mechanics of uniaxial strain.

1. We begin by formulating, and evaluating if possible, two dimensionless indefinite integrals:

$$\mathcal{I}_1(\phi_f) \equiv \frac{1}{k_0 \mathcal{M}} \int k(\phi_f) \frac{d\sigma'_{xx}}{d\phi_f} d\phi_f \quad \text{and} \quad (\text{D1a})$$

$$\mathcal{I}_2(\phi_f) \equiv \frac{1}{k_0 \mathcal{M}} \int \left(\frac{\phi_f - \phi_{f,0}}{1 - \phi_{f,0}} \right) k(\phi_f) \frac{d\sigma'_{xx}}{d\phi_f} d\phi_f. \quad (\text{D1b})$$

This relies on the fact that the effective stress can always be written directly in terms of the porosity in this geometry, $\sigma'_{xx} = \sigma'_{xx}(\phi_f)$ (see the discussion at the end of §IV B 2). For the elasticity and permeability laws considered above, we provide the results in Appendix F.

2. At steady state, we have that $v_s = 0$ and $\phi_f v_f = q^*$. The former statement with Equation (31c), or the latter statement with Equation (31b), leads to

$$q^* + \frac{k(\phi_f)}{\mu} \frac{\partial \sigma'_{xx}}{\partial x} = 0, \quad (\text{D2})$$

where we have replaced the pressure gradient with the effective stress gradient using Equation (31d). Equation (D2) can be rearranged and integrated to give

$$-\frac{\mu q^* L}{k_0 \mathcal{M}} \left(\frac{x}{L} - \frac{\delta^*}{L} \right) = \mathcal{I}_1(\phi_f(x)) - \mathcal{I}_1(\phi_f(\delta^*)), \quad (\text{D3})$$

where $\phi_f(\delta^*)$ is calculated from σ'^* by inverting $\sigma'_{xx}(\phi_f(\delta^*)) = \sigma'^*$. We next derive an expression for $u_s(x)$ using Equation (30), which can be rearranged using Equation (D2) and then integrated to give

$$\frac{u_s(x)}{L} = \frac{\delta^*}{L} - \frac{k_0 \mathcal{M}}{\mu q^* L} \left[\mathcal{I}_2(\phi_f(x)) - \mathcal{I}_2(\phi_f(\delta^*)) \right], \quad (\text{D4})$$

where we have applied the boundary condition that $u_s(\delta^*) = \delta^*$. Finally, we evaluate Equations (D3) and

(D4) at $x = L$ by applying the boundary condition that $u_s(L) = 0$, and rearranging to eliminate δ^* :

$$\left[\mathcal{I}_2(\phi_f(L)) - \mathcal{I}_2(\phi_f(\delta^*)) \right] - \left[\mathcal{I}_1(\phi_f(L)) - \mathcal{I}_1(\phi_f(\delta^*)) \right] = \frac{\mu q^* L}{k_0 \mathcal{M}}. \quad (\text{D5})$$

If Δp^* is known, $\phi_f(L)$ can be calculated by inverting $\sigma'_{xx}(\phi_f(L)) = \sigma'^* - \Delta p^*$. Equation (D5) then provides an explicit expression for q^* . If q^* is known instead, Equation (D5) provides an implicit expression for $\phi_f(L)$, which can then be used to calculate Δp^* from $\Delta p^* = \sigma'^* - \sigma'_{xx}(\phi_f(L))$.

3. Now that both q^* and Δp^* are known, δ^* can be calculated explicitly from Equation (D4) evaluated at $x = L$,

$$\frac{\delta^*}{L} = \frac{k_0 \mathcal{M}}{\mu q^* L} \left[\mathcal{I}_2(\phi_f(L)) - \mathcal{I}_2(\phi_f(\delta^*)) \right]. \quad (\text{D6})$$

4. Equation (D3) now provides an implicit expression for $\phi_f(x)$ in terms of q^* and δ^* .

5. Equation (D4) now provides an explicit expression for $u_s(x)$ in terms of q^* , δ^* , and $\phi_f(x)$.

6. Finally, the effective stress can be calculated from $\phi_f(x)$, and then the pressure from the effective stress,

$$\sigma'_{xx}(x) = \sigma'_{xx}(\phi_f(x)), \quad (\text{D7a})$$

$$p(x) = \sigma'_{xx}(x) - (\sigma'^* - \Delta p^*), \quad (\text{D7b})$$

where the latter comes from integrating Equation (31d) and applying the final boundary condition, $p(L) = 0$.

This procedure can be implemented analytically as long as the integrals can be evaluated exactly, although numerical root-finding is required in most cases. When the integrals cannot be evaluated exactly, it is straightforward to implement this numerically using standard quadrature techniques.

Appendix E: Steady-state solutions: Maximum values

The effective stress is always largest in magnitude at the right boundary ($x = L$), so this is where the porosity and permeability are the smallest, and the flow must stop when these vanish. Provided that σ'^* is known, this allows for the direct calculation of the maximum achievable values q_{\max}^* , Δp_{\max}^* , and δ_{\max}^* for which the porosity vanishes at $x = L$. The maximum flux q_{\max}^* can be evaluated directly from Equation (D5) by setting $\phi_f(L) = 0$,

$$\frac{\mu q_{\max}^* L}{k_0 \mathcal{M}} = \left[\mathcal{I}_2(0) - \mathcal{I}_2(\phi_f(\delta^*)) \right] - \left[\mathcal{I}_1(0) - \mathcal{I}_1(\phi_f(\delta^*)) \right]. \quad (\text{E1})$$

The maximum pressure drop Δp_{\max}^* can be evaluated directly from the elasticity law by setting $\phi_f(L) = 0$,

$$\Delta p_{\max}^* = \sigma'^* - \sigma'_{xx}(\phi_f = 0). \quad (\text{E2})$$

The maximum deflection δ_{\max}^* can be evaluated directly from Equation (D6) by setting $q^* = q_{\max}^*$ and $\phi_f(L) = 0$,

$$\frac{\delta_{\max}^*}{L} = \frac{k_0 \mathcal{M}}{\mu q_{\max}^* L} \left[\mathcal{I}_2(0) - \mathcal{I}_2(\phi_f(\delta^*)) \right]. \quad (\text{E3})$$

These three values occur simultaneously for a given σ'^* , and they are physical limits in the sense that it is not possible to drive a flux greater than q_{\max}^* or a deflection greater than δ_{\max}^* , or to apply a pressure drop greater than Δp_{\max}^* , without producing a negative porosity at the right boundary. Although solutions may exist for larger values, they will be non-physical.

Appendix F: Steady-state solutions: Integrals for specific cases

Here, we evaluate the integrals $\mathcal{I}_1(\phi_f)$ and $\mathcal{I}_2(\phi_f)$ (Equation D1) for the scenarios considered in §VIA above: Linear elasticity (for use with the intermediate model) and Hencky elasticity (for use with the nonlinear model), each for both constant permeability ($k = k_0$) and deformation-dependent permeability ($k = k(\phi_f)$) via the normalized Kozeny-Carman formula, Equation 12). In each case, we first write the elasticity law in terms of the porosity and then evaluate the first derivative of this function. For linear elasticity, we have

$$\frac{\sigma'_{xx}(\phi_f)}{\mathcal{M}} = \frac{\phi_f - \phi_{f,0}}{1 - \phi_{f,0}} \quad \text{and} \quad \frac{1}{\mathcal{M}} \frac{d\sigma'_{xx}}{d\phi_f} = \frac{1}{1 - \phi_{f,0}}. \quad (\text{F1})$$

For Hencky elasticity, we instead have

$$\frac{\sigma'_{xx}(\phi_f)}{\mathcal{M}} = \left(\frac{1 - \phi_f}{1 - \phi_{f,0}} \right) \ln \left(\frac{1 - \phi_{f,0}}{1 - \phi_f} \right) \quad \text{and} \quad (\text{F2a})$$

$$\frac{1}{\mathcal{M}} \frac{d\sigma'_{xx}}{d\phi_f} = \frac{1}{1 - \phi_{f,0}} \left[1 - \ln \left(\frac{1 - \phi_{f,0}}{1 - \phi_f} \right) \right]. \quad (\text{F2b})$$

We now evaluate the two integrals. These expressions can then be used with the procedure described in Appendix D to evaluate the full steady-state solutions for these constitutive models. Note that the integrals are indefinite, so arbitrary constants can be added or subtracted from the expressions below without loss of generality.

- intermediate- k_0 (linear elasticity with constant permeability)

$$\mathcal{I}_1(\phi_f) = \frac{\phi_f - \phi_{f,0}}{1 - \phi_{f,0}} \quad \text{and} \quad \mathcal{I}_2(\phi_f) = \frac{1}{2} \left(\frac{\phi_f - \phi_{f,0}}{1 - \phi_{f,0}} \right)^2 \quad (\text{F3})$$

- intermediate- k_{KC} (linear elasticity with normalized Kozeny-Carman permeability)

$$\mathcal{I}_1(\phi_f) = \frac{1 - \phi_{f,0}}{\phi_{f,0}^3} \left[\frac{1}{2} \phi_f^2 + 2\phi_f + \frac{1}{1 - \phi_f} + 3 \ln(1 - \phi_f) \right] \quad \text{and} \quad (\text{F4a})$$

$$\mathcal{I}_2(\phi_f) = \frac{1}{\phi_{f,0}^3} \left[-\frac{1}{3}(1 - \phi_f)^3 + \frac{1}{2}(4 - \phi_{f,0})(1 - \phi_f)^2 - 3(2 - \phi_{f,0})(1 - \phi_f) + \frac{1 - \phi_{f,0}}{1 - \phi_f} + (4 - 3\phi_{f,0}) \ln(1 - \phi_f) \right] \quad (\text{F4b})$$

- nonlinear- k_0 (Hencky elasticity with constant permeability)

$$\mathcal{I}_1(\phi_f) = \left(\frac{1 - \phi_f}{1 - \phi_{f,0}} \right) \ln \left(\frac{1 - \phi_{f,0}}{1 - \phi_f} \right) \quad \text{and} \quad (\text{F5a})$$

$$\mathcal{I}_2(\phi_f) = \frac{1}{4} \left(\frac{1 - \phi_f}{1 - \phi_{f,0}} \right)^2 + \frac{1}{2} \left[1 - \left(\frac{\phi_f - \phi_{f,0}}{1 - \phi_{f,0}} \right)^2 \right] \ln \left(\frac{1 - \phi_{f,0}}{1 - \phi_f} \right) \quad (\text{F5b})$$

- nonlinear- k_{KC} (Hencky elasticity with normalized Kozeny-Carman permeability)

$$\mathcal{I}_1(\phi_f) = \frac{1 - \phi_{f,0}}{4\phi_{f,0}^3} \left[\phi_f^2 + 2 \left(\frac{\phi_f^3 + 3\phi_f^2 - 4\phi_f - 2}{1 - \phi_f} \right) \ln \left(\frac{1 - \phi_{f,0}}{1 - \phi_f} \right) + 6 \ln^2 \left(\frac{1 - \phi_{f,0}}{1 - \phi_f} \right) - 2\phi_f + \frac{8}{1 - \phi_f} + 2 \ln(1 - \phi_f) \right] \quad (\text{F6a})$$

$$\mathcal{I}_2(\phi_f) = \frac{1}{36\phi_{f,0}^3} \left\{ 8\phi_f^3 + 3(4 - 3\phi_{f,0})\phi_f^2 - 6(8 - 3\phi_{f,0})\phi_f - 6(2 + 3\phi_{f,0}) \ln(1 - \phi_f) + 6 \left[\frac{2\phi_f^4 + (4 - 3\phi_{f,0})(3 + \phi_f)\phi_f^2 - 6(3 - 2\phi_{f,0})\phi_f - 6(1 - \phi_{f,0})}{1 - \phi_f} \right] \ln \left(\frac{1 - \phi_{f,0}}{1 - \phi_f} \right) + 72 \left(\frac{1 - \phi_{f,0}}{1 - \phi_f} \right) + 18(4 - 3\phi_{f,0}) \ln^2 \left(\frac{1 - \phi_{f,0}}{1 - \phi_f} \right) \right\} \quad (\text{F6b})$$

[1] V. C. Mow, S. C. Kuei, W. M. Lai, and C. G. Armstrong, “Biphasic creep and stress relaxation of articular cartilage in compression: Theory and experiments,” *Journal of Biomechanical Engineering* **102**, 73–84 (1980).
[2] W. M. Lai, J. S. Hou, and V. C. Mow, “A triphasic theory for the swelling and deformation behaviors of articular cartilage,” *Journal of Biomechanical Engineering* **113**, 245–258 (1991).
[3] M. Yang and L. A. Taber, “The possible role of proe-

lasticity in the apparent viscoelastic behavior of passive cardiac muscle,” *Journal of Biomechanics* **24**, 587–597 (1991).
[4] S. C. Cowin, “Bone poroelasticity,” *Journal of Biomechanics* **32**, 217–238 (1999).
[5] G. Franceschini, D. Bigoni, P. Regitnig, and G. A. Holzapfel, “Brain tissue deforms similarly to filled elastomers and follows consolidation theory,” *Journal of the Mechanical and Physics of Solids* **54**, 2592–2620 (2006).

- [6] J. M. Skotheim and L. Mahadevan, “Physical limits and design principles for plant and fungal movements,” *Science* **308**, 1308–1310 (2005).
- [7] G. T. Charras, J. C. Yarrow, M. A. Horton, L. Mahadevan, and T. J. Mitchison, “Non-equilibration of hydrostatic pressure in blebbing cells,” *Nature* **435**, 365–369 (2005).
- [8] J. Dumais and Y. Forterre, “‘Vegetable Dynamicks’: The role of water in plant movements,” *Annual Review of Fluid Mechanics* **44**, 453–478 (2012).
- [9] E. Moeendarbary, L. Valon, M. Fritzsche, A. R. Harris, D. A. Moulding, A. J. Thrasher, E. Stride, L. Mahadevan, and G. T. Charras, “The cytoplasm of living cells behaves as a poroelastic material,” *Nature Materials* **12**, 253–261 (2013).
- [10] D. McKenzie, “The generation and compaction of partially molten rock,” *Journal of Petrology* **25**, 713–765 (1984).
- [11] A. C. Fowler, “A mathematical model of magma transport in the asthenosphere,” *Geophysical & Astrophysical Fluid Dynamics* **33**, 63–96 (1985).
- [12] M. Spiegelman, “Flow in deformable porous media. Part 1. Simple analysis,” *Journal of Fluid Mechanics* **247**, 17–38 (1993).
- [13] D. Bercovici, Y. Ricard, and G. Schubert, “A two-phase model for compaction and damage 1. General theory,” *Journal of Geophysical Research* **106**, 8887–8906 (2001).
- [14] R. F. Katz, “Magma dynamics with the enthalpy method: Benchmark solutions and magmatic focusing at mid-ocean ridges,” *Journal of Petrology* **49**, 2099–2121 (2008).
- [15] M. A. Hesse, A. R. Schiemenz, Y. Liang, and E. M. Parmentier, “Compaction-dissolution waves in an upwelling mantle column,” *Geophysical Journal International* **187**, 1057–1075 (2011).
- [16] J. Bear and M. Y. Corapcioglu, “Mathematical model for regional land subsidence due to pumping: 1. Integrated aquifer subsidence equations based on vertical displacement only,” *Water Resources Research* **17**, 937–946 (1981).
- [17] H. F. Wang, *Theory of Linear Poroelasticity* (Princeton University Press, Princeton NJ, 2000).
- [18] M. L. Szulczewski, C. W. MacMinn, H. J. Herzog, and R. Juanes, “Lifetime of carbon capture and storage as a climate-change mitigation technology,” *Proceedings of the National Academy of Sciences of the United States of America* **109**, 5185–5189 (2012).
- [19] J. Rutqvist, “The geomechanics of CO₂ storage in deep sedimentary formations,” *Geotechnical and Geological Engineering* **30**, 525–551 (2012).
- [20] K. W. Chang, M. A. Hesse, and J.-P. Nicot, “Reduction in lateral pressure propagation due to dissipation into ambient mudrocks during geological carbon dioxide storage,” *Water Resources Research* **49**, 2573–2588 (2013).
- [21] J. P. Verdon, J.-M. Kendall, A. L. Stork, R. A. Chadwick, D. J. White, and R. C. Bissell, “Comparison of geomechanical deformation induced by megatonne-scale CO₂ storage at Sleipner, Weyburn, and In Salah,” *Proceedings of the National Academy of Sciences of the United States of America* **110**, E2762–71 (2013).
- [22] V. M. Yarushina, D. Bercovici, and M. L. Oristaglio, “Rock deformation models and fluid leak-off in hydraulic fracturing,” *Geophysical Journal International* **194**, 1514–1526 (2013).
- [23] B. Jha and R. Juanes, “Coupled multiphase flow and poromechanics: A computational model of pore-pressure effects on fault slip and earthquake triggering,” *Water Resources Research* **50**, 3776–3808 (2014).
- [24] Z. Cai and D. Bercovici, “Two-phase viscoelastic damage theory, with applications to subsurface fluid injection,” *Geophysical Journal International* **199**, 1481–1496 (2014).
- [25] D. R. Hewitt, J. A. Neufeld, and N. J. Balmforth, “Shallow, gravity-driven flow in a poro-elastic layer,” *Journal of Fluid Mechanics* **778**, 335–360 (2015).
- [26] R. de Boer, “Highlights in the historical development of the porous media theory: Toward a consistent macroscopic theory,” *Applied Mechanics Reviews* **49**, 201–262 (1996).
- [27] M. A. Biot, “General theory of three-dimensional consolidation,” *Journal of Applied Physics* **12**, 155–164 (1941).
- [28] M. A. Biot, “Theory of propagation of elastic waves in a fluid-saturated porous solid. I. Low-frequency range,” *Journal of the Acoustical Society of America* **28**, 168–178 (1956).
- [29] M. A. Biot, “Mechanics of deformation and acoustic propagation in porous media,” *Journal of Applied Physics* **33**, 1482 (1962).
- [30] J. R. Rice and M. P. Cleary, “Some basic stress diffusion solutions for fluid-saturated elastic porous media with compressible constituents,” *Reviews of Geophysics and Space Physics* **14**, 227–241 (1976).
- [31] M. A. Biot, “Theory of finite deformations of porous solids,” *Indiana University Mathematics Journal* **21**, 597–620 (1972).
- [32] O. Coussy, *Poromechanics* (Wiley, 2004).
- [33] M. H. Holmes and V. C. Mow, “The nonlinear characteristics of soft gels and hydrated connective tissues in ultrafiltration,” *Journal of Biomechanics* **23**, 1145–1156 (1990).
- [34] M. K. Kwan, W. M. Lai, and V. C. Mow, “A finite deformation theory for cartilage and other soft hydrated connective tissues—I. equilibrium results,” *Journal of Biomechanics* **23**, 145–155 (1990).
- [35] B. R. Simon, “Multiphase poroelastic finite element models for soft tissue,” *Applied Mechanics Reviews* **45**, 191–218 (1992).
- [36] M. Argoubi and A. Shirazi-Adl, “Poroelastic creep response analysis of a lumbar motion segment in compression,” *Journal of Biomechanics* **29**, 1331–1339 (1996).
- [37] S. Federico and A. Grillo, “Elasticity and permeability of porous fibre-reinforced materials under large deformations,” *Mechanics of Materials* **44**, 58–71 (2012).
- [38] A. Tomic, A. Grillo, and S. Federico, “Poroelastic materials reinforced by statistically oriented fibers—numerical implementation and applications to articular cartilage,” *IMA Journal of Applied Mathematics* **79**, 1027–1059 (2014).
- [39] A.-T. Vuong, L. Yoshihara, and W. A. Wall, “A general approach for modeling interacting flow through porous media under finite deformations,” *Computer Methods in Applied Mechanics and Engineering* **283**, 1240–1259 (2015).
- [40] J. P. Carter, J. R. Booker, and J. C. Small, “The analysis of finite elasto-plastic consolidation,” *International Journal for Numerical and Analytical Methods in Geomechanics* **3**, 107–129 (1979).
- [41] R. I. Borja and E. Alarcón, “A mathematical framework

- for finite strain elastoplastic consolidation. part 1: Balance laws, variational formulation, and linearization,” *Computer Methods in Applied Mechanics and Engineering* **122**, 145–171 (1995).
- [42] C. Li, R. I. Borja, and R. A. Regueiro, “Dynamics of porous media at finite strain,” *Computer Methods in Applied Mechanics and Engineering* **193**, 3837–3870 (2004).
- [43] R. Uzuoka and R. I. Borja, “Dynamics of unsaturated poroelastic solids at finite strain,” *International Journal for Numerical and Analytical Methods in Geomechanics* **36**, 1535–1573 (2011).
- [44] L. S. Bennethum and J. H. Cushman, “Multiscale, hybrid mixture theory for swelling systems—I: Balance laws,” *International Journal of Engineering Science* **34**, 125–145 (1996).
- [45] J. M. Huyghe and J. D. Janssen, “Quadriphasic mechanics of swelling incompressible porous media,” *International Journal of Engineering Science* **35**, 793–802 (1997).
- [46] W. Hong, X. Zhao, J. Zhou, and Z. Suo, “A theory of coupled diffusion and large deformation in polymeric gels,” *Journal of the Mechanics and Physics of Solids* **56**, 1779–1793 (2008).
- [47] F. P. Duda, A. C. Souza, and E. Fried, “A theory for species migration in a finitely strained solid with application to polymer network swelling,” *Journal of the Mechanical and Physics of Solids* **58**, 515–529 (2010).
- [48] S. A. Chester and L. Anand, “A coupled theory of fluid permeation and large deformations for elastomeric materials,” *Journal of the Mechanics and Physics of Solids* **58**, 1879–1906 (2010).
- [49] S. M. Hassanizadeh and W. G. Gray, “General conservation equations for multi-phase systems: 1. Averaging procedure,” *Advances in Water Resources* **2**, 131–144 (1979).
- [50] L. S. Bennethum, “Compressibility moduli for porous materials incorporating volume fraction,” *Journal of Engineering Mechanics* **132**, 1205–1214 (2006).
- [51] J. C. Jaeger, N. G. W. Cook, and R. Zimmerman, *Fundamentals of Rock Mechanics*, 4th ed. (Wiley-Blackwell, 2007) ISBN: 978-0-632-05759-7.
- [52] A. Gajo, “A general approach to isothermal hyperelastic modelling of saturated porous media at finite strains with compressible solid constituents,” *Proceedings of the Royal Society A* **466**, 3061–3087 (2010).
- [53] J. E. Marsden and T. J. R. Hughes, *Mathematical foundations of elasticity* (Dover Publications, Inc., New York, 1983) ISBN 0-486-67865-2. Available at <http://resolver.caltech.edu/CaltechBOOK:1983.002>.
- [54] M. E. Gurtin, E. Fried, and L. Anand, *The Mechanics and Thermodynamics of Continua* (Cambridge University Press, 2010).
- [55] R. B. Bird, R. C. Armstrong, and O. Hassager, *Dynamics of Polymer Liquids, Volume 1: Fluid Mechanics* (Wiley-Interscience, 1987).
- [56] R. B. Bird, C. F. Curtiss, R. C. Armstrong, and O. Hassager, *Dynamics of Polymer Liquids, Volume 2: Kinetic Theory* (Wiley-Interscience, 1987).
- [57] G. F. Pinder and W. G. Gray, *Essentials of multiphase flow in porous media* (Wiley-Interscience, Hoboken, NJ, USA, 2008).
- [58] Y.-S. Wu and K. Pruess, “Flow of non-Newtonian fluids in porous media,” in *Advances in Porous Media*, Vol. 3 (Elsevier, 1996) Chap. 2, pp. 87–184.
- [59] K. von Terzaghi, “The shearing resistance of saturated soil and the angle between the planes of shear,” in *Proceedings of the International Conference on Soil Mechanics and Foundation Engineering, June 22 to 26*, Vol. 1 (1936) pp. 54–56.
- [60] A. Nur and J. D. Byerlee, “An exact effective stress law for elastic deformation of rock with fluids,” *Journal of Geophysical Research* **76**, 6414–6419 (1971).
- [61] L. Anand, “On H. Hencky’s approximate strain-energy function for moderate deformations,” *Journal of Applied Mechanics* **46**, 78–82 (1979).
- [62] H. Xiao and L. S. Chen, “Hencky’s elasticity model and linear stress-strain relations in isotropic finite hyperelasticity,” *Acta Mechanica* **157**, 51–60 (2002).
- [63] L. Anand, “Moderate deformations in extension-torsion of incompressible isotropic elastic materials,” *Journal of the Mechanics and Physics of Solids* **34**, 293–304 (1986).
- [64] Z. P. Bažant, “Easy-to-compute tensors with symmetric inverse approximating Hencky finite strain and its rate,” *Journal of Engineering Materials and Technology* **120**, 131–136 (1998).
- [65] G. S. Beavers and D. D. Joseph, “Boundary conditions at a naturally permeable wall,” *Journal of Fluid Mechanics* **30**, 197–207 (1967).
- [66] U. Shavit, “Special Issue on ‘Transport phenomena at the interface between fluid and porous domains’,” *Transport in Porous Media* **78**, 327–330 (2009).
- [67] K. Mosthaf, K. Baber, B. Flemisch, R. Helmig, A. Leijnse, I. Rybak, and B. Wohlmuth, “A coupling concept for two-phase compositional porous-medium and single-phase compositional free flow,” *Water Resources Research* **47**, W10522 (2011).
- [68] S. I. Barry and G. K. Aldis, “Comparison of models for flow induced deformation of soft biological tissue,” *Journal of Biomechanics* **23**, 647–654 (1990).
- [69] S. I. Barry and G. K. Aldis, “Unsteady flow induced deformation of porous materials,” *International Journal of Non-Linear Mechanics* **26**, 687–699 (1991).
- [70] L. Preziosi, D. D. Joseph, and G. S. Beavers, “Infiltration of initially dry, deformable porous media,” *International Journal of Multiphase Flow* **22**, 1205–1222 (1996).
- [71] M. H. Holmes, “Finite deformation of soft tissue: Analysis of a mixture model in uni-axial compression,” *Journal of Biomechanical Engineering* **108**, 372–381 (1986).
- [72] M. A. Dawson, G. H. McKinley, and L. J. Gibson, “The dynamic compressive response of an open-cell foam impregnated with a Newtonian fluid,” *Journal of Applied Mechanics* **75**, 041015 (2008).
- [73] J. L. Sommer and A. Mortensen, “Forced unidirectional infiltration of deformable porous media,” *Journal of Fluid Mechanics* **311**, 193–217 (1996).
- [74] D. M. Anderson, “Imbibition of a liquid droplet on a deformable porous substrate,” *Physics of Fluids* **17**, 087104 (2005).
- [75] J. I. Siddique, D. M. Anderson, and A. Bondarev, “Capillary rise of a liquid into a deformable porous material,” *Physics of Fluids* **21**, 013106 (2009).
- [76] G. S. Beavers, A. Hajji, and E. M. Sparrow, “Fluid flow through a class of highly-deformable porous media. Part I: Experiments with air,” *Journal of Fluids Engineering* **103**, 432 (1981).
- [77] G. S. Beavers, K. Wittenberg, and E. M. Sparrow, “Fluid flow through a class of highly-deformable porous media. Part II: Experiments with water,” *Journal of Fluids Engineering* **103**, 440 (1981).
- [78] K. H. Parker, R. V. Mehta, and C. G. Caro, “Steady

- flow in porous, elastically deformable materials,” *Journal of Applied Mechanics* **54**, 794 (1987).
- [79] See Supplemental Material at [URL will be inserted by publisher] for a **MATLAB** implementation of the models, solutions, and results presented in §IV–VI.
- [80] G. S. Beavers, T. A. Wilson, and B. A. Masha, “Flow through a deformable porous material,” *Journal of Applied Mechanics* **42**, 598–602 (1975).
- [81] A. Oloyede and N. D. Broom, “Is classical consolidation theory applicable to articular cartilage deformation?” *Clinical Biomechanics* **6**, 206–212 (1991).
- [82] M. A. Murad, L. S. Bennethum, and J. H. Cushman, “A multi-scale theory of swelling porous media: I. Application to one-dimensional consolidation,” *Transport in Porous Media* **19**, 93–122 (1995).
- [83] R. Lancellotta and L. Preziosi, “A general nonlinear mathematical model for soil consolidation problems,” *International Journal of Engineering Science* **35**, 1045–1063 (1997).
- [84] Y. Lanir, S. Sauob, and P. Maretsky, “Nonlinear finite deformation response of open cell polyurethane sponge to fluid filtration,” *Journal of Applied Mechanics* **57**, 449 (1990).
- [85] B. Sobac, M. Colombani, and Y. Forterre, “On the dynamics of poroelastic foams (*in French*),” *Mécanique & Industries* **12**, 231–238 (2011).
- [86] D. R. Hewitt, J. S. Nijjer, M. G. Worster, and J. A. Neufeld, “Flow-induced compaction of a deformable porous medium,” *Physical Review E* **93**, 023116 (2016).
- [87] R. J. LeVeque, *Finite-volume methods for hyperbolic problems* (Cambridge University Press, 2004).
- [88] S. I. Barry and G. K. Aldis, “Radial flow through deformable porous shells,” *Journal of the Australian Mathematical Society. Series B. Applied Mathematics* **34**, 333–354 (1993).